Project Title: **Investigating Lateral Buckling of Joists as a Cause of Falls from Elevation**

PI and Project Director: Daniel P. Hindman, Associate Professor
Department of Wood Science and Forest Products
1650 Ramble Road
Blacksburg, VA 24061
(540) 231-9442
dhindman@vt.edu

Co-Investigators: Maury A. Nussbaum
Professor
Department of Industrial Systems Engineering
Virginia Polytechnic Institute and State University

Awarding Institution: Virginia Polytechnic Institute and State University
Office of Sponsored Programs
1880 Pratt Drive
Suite 2006 (MC 0170)
Blacksburg, Virginia 24060
(Ph) 540-231-5281 (Fax) 540-231-3599

Department of Health and Human Services Public Health Services	Review Group	Type	Activity	Grant Number R21 OH 008902-02	

Grant Progress Report

Total Project Period
From: 8/1/2007   Through: 7/31/2010
Requested Budget Period
From: Through:

1. **TITLE OF PROJECT**
Investigating Lateral Buckling of Joists as a Cause of Falls from Elevation

2a. PROGRAM DIRECTOR / PRINCIPAL INVESTIGATOR (Name and address, street, city, state, zip code) Dr Daniel Hindman Virginia Polytechnic Institute & State University Dept of Wood Science & Forest Products 1650 Ramble Road Blacksburg, VA 24060	2b. E-MAIL ADDRESS dhindman@vt.edu
	2c. DEPARTMENT, SERVICE, LABORATORY, OR EQUIVALENT Dept of Wood Science & Forest Porducts
	2d. MAJOR SUBDIVISION
	2e. Tel: 540-231-9442 Fax:

3a. APPLICANT ORGANIZATION (Name and address, street, city, state, zip code) Virginia Polytechnic Institute & State University 1880 Pratt Drive, Suite 2006 Blacksburg, VA 24060	3b. Tel: 540-231-5281 Fax: 540-231-3599
	3c. DUNS: 003137015

4. **ENTITY IDENTIFICATION NUMBER**
54-6001805

6. HUMAN SUBJECTS ☐ No ☒ Yes	5. NAME, TITLE AND ADDRESS OF ADMINISTRATIVE OFFICIAL
6a. Research Exempt ☒ No ☐ Yes	John Rudd, Asst. VP for Sponsored Programs Virginia Polytechnic Institute & State University 1880 Pratt Drive, Suite 2006
If Exempt ("Yes" in 6a): Exemption No.	
If Not Exempt ("No" in 6a): IRB approval date	
6b. Federal Wide Assurance No. FWA00000572	Tel: 540-231-5281 Fax: 540-231-3599
6c. NIH-Defined Phase III Clinical Trial ☒ No ☐ Yes	E-MAIL: bakerjj@vt.edu

7. VERTEBRATE ANIMALS ☒ No ☐ Yes	10. PROJECT/PERFORMANCE SITE(S)
7a. If "Yes," IACUC approval Date	Organizational Name: Virginia Polytechnic Inst & State Univer.
7b. Animal Welfare Assurance No.	DUNS: 003137015

8. COSTS REQUESTED FOR NEXT BUDGET PERIOD	Street 1:
8a. DIRECT $ 8b. TOTAL $	Street 2:

9. INVENTIONS AND PATENTS ☐ No ☒ Yes	City: Blacksburg	County:
If "Yes," ☒ Previously Reported ☐ Not Previously Reported	State: VA	Province:
	Country: USA	Zip/Postal Code: 24060
	Congressional Districts: 9th	

11. **NAME AND TITLE OF OFFICIAL SIGNING FOR APPLICANT ORGANIZATION** *(Item 13)*
John Rudd, Asst. VP for Sponsored Programs

TEL: 540-231-5281	FAX: 540-531-3599	E-MAIL: bakerjj@vt.edu

12. Corrections to Page 1 Face Page

13. APPLICANT ORGANIZATION CERTIFICATION AND ACCEPTANCE: I certify that the statements herein are true, complete and accurate to the best of my knowledge, and accept the obligation to comply with Public Health Services terms and conditions if a grant is awarded as a result of this application. I am aware that any false, fictitious, or fraudulent statements or claims may subject me to criminal, civil, or administrative penalties.	SIGNATURE OF OFFICIAL NAMED IN 11. *(In ink)*	DATE 10/27/2010

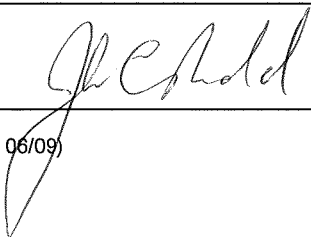| Department of Health and Human Services **Final Invention Statement and Certification** *(For Grant or Award)*	DHHS Grant or Award No. 5R21OH008902-02

A. We hereby certify that, to the best of our knowledge and belief, all inventions are listed below which were conceived and/or first actually reduced to practice during the course of work under the above-referenced DHHS grant or award for the period

08/01/2007	through	07/31/2010	.
original effective date		*date of termination*	

B. Inventions (Note: If no inventions have been made under the grant or award, insert the word *"NONE"* under Title below.)

NAME OF INVENTOR	TITLE OF INVENTION	DATE REPORTED TO DHHS
Daniel Hindman	Temp. Stabilizer for Wood Joist Installation	04/21/08

(Use continuation sheet if necessary)

C. Signature — This block *must* be signed by an official authorized to sign on behalf of the institution.

Title Asst. VP of Sponsored Programs	Name and Mailing Address of Institution Virginia Polytechnic Institute and State University Office of Sponsored Programs 1880 Pratt Drive, Suite 2006 Blacksburg, VA 24060
Typed Name John C Rudd	

Signature	Date 10/27/10	

HHS 568 (Rev. 06/09)

FINANCIAL STATUS REPORT

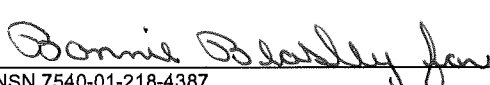*(Short Form)*

(Follow instructions on the back)

1. Federal Agency and Organizational Element to Which Report is Submitted NAT INST FOR OCCUP. SAFETY & HEALTH	2. Federal Grant or Other Identifying Number Assigned By Federal Agency R21 OH008902-02	OMB Approval No. **0348-0038**	Page of pages

3. Recipient Organization (Name and complete address, including ZIP code)
Virginia Polytechnic Institute & State Univ., Office of Sponsored Programs, 1880 Pratt Drive, Ste 2006, Blacksburg, VA 24060

4. Employer Identification Number 54-6001805	5. Recipient Account Number or Identifying Number 431515	6. Final Report ☒ Yes ☐ No	7. Basis ☒ Cash ☐ Accrual

8. Funding/Grant Period *(See instructions)*		9. Period Covered by this Report	
From: (Month, Day, Year) 8/1/2007	To: (Month, Day, Year) 7/31/2010	From: (Month, Day, Year) 8/1/2007	To: (Month, Day, Year) 7/31/2010

10. Transactions:	I Previously Reported	II This Period	III Cumulative
a. Total outlays	0	388,631.27	388,631.27
b. Recipient share of outlays	0		
c. Federal share of outlays	0	388,631.27	388,631.27
d. Total unliquidated obligations			
e. Recipient share of unliquidated obligations			
f. Federal share of unliquidated obligations			
g. Total Federal share *(Sum of lines c and f)*			
h. Total Federal funds authorized for this funding period			
i. Unobligated balance of Federal funds *(Line h minus line g)*			

11. Indirect Expense	a. Type of Rate *(Place "X" in appropriate box)* ☐ Provisional ☐ Predetermined ☐ Final ☒ Fixed			
	b. Rate 51%	c. Base 205,833	d. Total Amount 104,975	e. Federal Share 104,975

12. *Remarks: Attach any explanations deemed necessary or information required by Federal sponsoring agency in compliance with governing legislation.*

13. Certification: I certify to the best of my knowledge and belief that this report is correct and complete and that all outlays and unliquidated obligations are for the purposes set forth in the award documents.

Typed or Printed Name and Title John Rudd, Asst. VP for Sponsored Programs	Telephone (Area code, number and extension) 540-231-5281
Signature of Authorized Certifying Official 	Date Report Submitted 11/1/2010

Table of Contents

List of Abbreviations and Terms

Lateral buckling – stability phenomenon when a loaded unbraced beam experiences lateral deflection (to the side) and twist

Wood composite I-joists – a structural wood member in the shape of a capital I. The top and bottom of the I (flanges) are composed of solid wood or LVL, and the center of the I (web) is composed of OSB or plywood

SCL – structural composite lumber – a group of structural wood composites used in buildings to replace lumber products since most of the strength is in the longitudinal direction of the beam

LVL – laminated veneer lumber – an SCL material composed of bonded veneers of wood aligned parallel to the grain

OSB – oriented strandboard – a cross-ply wood composite composed of small wood strands bonded together to create a panel product having strength in both the parallel and perpendicular to grain directions

CBL – critical buckling load – for static loading, the load which causes the initiation of lateral buckling

FEM – finite element method – a numerical modeling tool using a set of matrices to solve for the loading, displacement and stiffness of a wood structural system

Lateral Acceleration – the amount of acceleration perpendicular to the length of the joist caused by workers walking along the joist

Lateral Displacement – the amount of deflection perpendicular to the length of the joist caused by workers walking along the joist

Twist - the amount of rotation of the joist cross-section about the longitudinal axis of the joist caused by workers walking along the joist

Abstract

Falls from elevation represent one of the most common construction safety incidents in residential construction. The focus of most previous fall-related research has been somewhat vague in the definition of the causes of falls as well as specific remediation. This research project investigated a particular fall mechanism – the lateral buckling of unbraced joists, particularly wood composite I-joists. The goal of this research was to explore the relationship between construction worker loadings and the mechanical behavior that causes lateral buckling of wood composite I-joists. This research project was novel in the study of a particular fall related mechanism, namely lateral buckling, which has not received much research interest. Intensive study of lateral buckling situations allowed researchers to formulate prevention strategies to enable workers to complete their task while reducing the occurence of lateral buckling.

Lateral buckling occurs in unbraced joists when a vertical load is applied. If the load is greater than the critical buckling load, the joist begins to deflect laterally (perpendicular to the length) and twist. When a dynamic load such as a person walking along the joist exceeds the critical buckling load, the joist can also begin to sway and wobble. As the worker moves towards the center of the joist, the amplitude of this sway and wobble become larger, possibly serving as the impetus for a loss of balance or fall. Many accident reports are nonspecific and give little evidence to help determine the root cause of falls, especially when lateral buckling is involved. Lateral buckling could easily be attributed to worker error or a slippery surface. Since lateral buckling is largely a stability concern with the joist, if the load is removed (i.e., worker steps off or falls), the joist returns to its initial position with no evidence that anything has happened. Lateral buckling occurs with all wood and wood composite beams as well as cold formed steel sections used in construction. Wood composite I-joists were chosen for this study as an example material due to the PI's familiarity and the tendency of the I-joists to buckle.

This research used a P2R2P (practice to research to practice) approach to accomplish the specific aims. The first practice was the observation of construction workers walking on unbraced joists during their tasks. Special attention was provided to the position, and the amount of tools and materials carried. Observation of worker loadings demonstrated the need for workers to walk on unbraced I-joists. Typically, workers were observed with tool belts and off-center loads of materials and tools.

Measurements of both the static and dynamic loading of the I-joists were conducted. Static loading used a point load applied at the mid-span of the I-joist using a specially designed loading fixture to eliminate any bracing effects. This testing examined the variability of load readings from the I-joists. Test subjects walking on a safety platform experienced lateral buckling behavior of the I-joists. Loading results indicated that the lateral load force applied to the I-joist by a worker walking varied from 9.3% to 72% of the test subject's static weight. This lateral load was greater than previous studies which had documented the lateral load associated with workers walking on a flat surface. Increased lateral load poses a particular problem in lateral buckling in that this tends to decrease the vertical load component at which buckling occurs.

A finite element model was constructed using a pseudo-dynamic loading method. For two of the three I-joist types, the I-joist movement was predicted to within a cumulative error of 10% until the test subject reached the mid-span of the beam. The loading data for the test subject walking after mid-span was dominated by secondary vibrations and could not be predicted. A

deterministic model was also presented which included the end support conditions and stiffness of bracing elements, but was not validated.

   To remediate lateral buckling, this research created a temporary joist stabilizer. This stabilizer could be used by workers to latch onto the joists in front of them creating a safe walking area. As work progressed along the length of the I-joists, the temporary brace could be moved to a new position. There is little to no research available on the movement of joists in partial bracing situations. To examine the amount of bracing stiffness and spacing needed, a second walking study was conducted using the safety platform. Braces of five different stiffness and two different spacing along the I-joist were tested. Bracing stiffness was found to be a more important factor than the bracing spacing to reduce the joist movement. Lateral displacement and twist of the joist increased as the test subject's static weight increased, while lateral acceleration did not change. This project provides the knowledge and background study needed to pursue the temporary joist stabilizer as a new invention to help workers avoid situations where joists may become unstable. Future plans include the production and development of this stabilizer as well as further testing and validation of the final product.

SECTION 1

Highlights / Significant Findings

Experimental Testing of Lateral Buckling

- A study of bracing effectiveness showed that the stiffness of bracing elements was more important than the spacing. This finding can confirm the use of less bracing and the use of the temporary joist stabilizer intellectual property as a viable tool to prevent lateral buckling.
- An optimal bracing stiffness may be the most cost effective choice based on the non-linear relationship of brace stiffness and joist movement.
- Studies of the test subjects walking showed that participant weight affected the lateral displacement and twist but had little change on the lateral acceleration of the I-joist. This is one of the few studies that has observed and documented joist movement as a function of bracing.

Modeling of Lateral Buckling

- A finite element model was developed to describe the joist motion of an unbraced wood composite I-joist undergoing a human walking load and experiencing lateral buckling.
- These models can be applied to other wood and cold-formed steel products given the input loading and joist stiffness properties.

Safety Platform for Measuring Loads

- A safety platform was constructed to measure lateral buckling movement of joists without exposing workers to fall hazards.
- Future use of this safety platform can study fall phenomena in the laboratory related to lateral buckling or other fall mechanisms.
- This platform has also been used as a demonstration piece for several classes and short courses to discuss the issues associated with worker falls from elevation and the interaction of wood material properties and safety considerations.

Observations of Construction Workers

- Observation of construction workers was coupled with laboratory measurements demonstrated that workers are exposed to lateral buckling hazards. Workers are exposed to off-center loading of their person by the presence of tools and materials which should be accounted for in research.

Translation of Findings

This research project has led to the creation of two Masters of Science (M.S.) theses available on the Virginia Tech website as well as several proceedings articles and presentations. Currently, four peer-reviewed journal publications are being written about this project and will be submitted before the end of 2010.

These journal publications provide safety professionals and civil engineers with recommendations on developing bracing guidelines to prevent lateral buckling during construction. The models developed in this research can be used to perform calculations to aid in choice of bracing on construction sites. The models will also be useful as a source for the input of movement into biomechanics research including slip plate studies of workers on beams. Bracing information in the papers and theses can be directly translated to construction sites because of the use of typical joist materials and spans.

Outcomes / Relevance / Impact

The greatest impact of this study is to demonstrate a direct approach to research related to the remediation of falls on construction sites. By studying proposed fall mechanisms, the direct relationship between falls and human loadings can be observed. This model can be expanded on by other researchers and result in a more directed focus to address the root causes of falls from elevation.

Another important impact of this project is the recognition that workers can experience lateral buckling of unbraced joists. Previous anecdotal evidence of this behavior was available with no direct measurement of lateral buckling. This study measured the movement of I-joists under lateral buckling, which has not been discussed in previous lateral buckling studies that were focused on beam capacity. This project measured and reported the lateral displacement, twist and lateral acceleration of the joist due to lateral buckling.

This study provides important information on the beam response and loading due to human walking loads on construction sites. This research could be coupled with future biomechanics studies to determine the limits of lateral acceleration, lateral displacement and twist which humans standing on a joist can endure before falls occur to develop the limits or further recommendations to prevent lateral buckling.

SECTION 2

Scientific Report

Background

Falls from elevation are one of the most prevalent accident types among construction workers. According to a Bureau of Labor Statistics (BLS) survey of occupational fatalities for 2004 (BLS 2004a), 14% of all workplace fatalities were caused by falls. Between 1992 and 2004, the number of falls reported by the BLS varied between 600 to 815 per year, with a general increase from 1992 to 2001, and the largest number of falls occurring in 2004 (BLS 2004a). In 2004, 54.1% of all fatal falls occurred in the construction field and 88.2% of all fatal falls recorded by the BLS from roofs occurred in the construction field (BLS 2004b). Falls from elevation represent 36.0% of the total number of fatalities among construction workers (BLS 2004c).

While falls from elevation cause many fatalities, the number of injuries and associated costs are also substantial. In a study of wood-frame residential construction workers in Washington state, Shah et al. (2003) found that 35.1% of all injuries were due to falls from elevation. Injuries from falls in construction result in twice the lost work time needed to recover compared to lost work time associated with falls in other industries (OSHA 1996). Lipscomb et al. (2003) noted that the average costs for a fall from elevation were $5664 for medical, $2243 for permanent impairment, and $9480 for lost time, resulting in an average cost of $17,387 per fall. In another study, Lipscomb et al. (2003b) found that falls from elevation dominated the costs of injuries among residential carpenters. Further, the indirect costs of injuries (including intangibles from the contractor and project) can be 4.2 times higher than the direct costs (Janicak 1997). Effective reduction of injuries caused by falls from elevation serves to protect the workforce, but also represents a significant cost savings to the construction industry in general.

Falls in the construction industry represent a major safety hazard that must be addressed. One population most at risk is roofers, especially in low-cost or residential construction (Lipscomb et al. 2003b and Janicak 1997). Huang and Hinze (2003) characterized the largest number of falls from elevation as occurring from 30 ft or less (typical height associated with residential construction). Richardson et al. (2004) and Hunting et al. (1994) indicate that males of Hispanic ethnicity represent a disproportionately high number of fall victims. These at-risk populations of residential construction workers, especially roofers, have received little attention.

Several studies have employed other technical methods to understand the physical mechanisms of balance and worker falls. Hsiao and Simenov (2001) used a biomechanical and psychophysical approaches to assess the causes of falls. Falls were concluded to be essentially loss of balance incidents, which can be caused by changes in the roof properties, among other issues. Maki et al. (1996) noted that if a perturbation caused a loss of balance, a person compensated with a stepping response. Lateral perturbations required 70% more recovery time than sagittal perturbations, so that any lateral motion of the roofing elements had a greater impact on a worker's balance.

Safety alerts and various intervention programs have been used to educate construction workers about the dangers posed by falls from elevation. NIOSH has initiated many alerts and web publications (NIOSH 1989, 2001, 2000) targeted towards specific occupational hazards related to falls from elevations. Rivara and Thompson (2000) examined the effectiveness of

three different fall protection programs. Many intervention methods do not contain studied observations of their ability to prevent falls. Rivara and Thompson (2000) recommended that future research efforts in this area focus on the application of theory and observation to understand fall prevention mechanisms.

The preceding paragraphs have discussed the problems associated with falls from elevation, especially among the roofing trades in residential construction. These falls present serious problems to worker health and project cost. The survey efforts which have been performed on many worksites present general observations of the fall events, but contain little if any significant information on the root causes of the falls. Though prevention programs and fall arrest devices are commonly used, there are still a large number of fall incidents occurring. Rivara and Thompson (2000) discussed the fact that little research has focused on the mechanics of falls in order to increase prevention efforts. One possible fall mechanism which may cause falls from roofing systems is **lateral buckling**, especially during construction situations when little or no bracing of load-bearing beam elements exists. Recent research has been conducted by Dr. Hindman to facilitate the general understanding of this stability phenomenon. **The purpose of the proposed project is to expand the understanding of lateral buckling as a cause of falls from elevation from unbraced structural beam members and ultimately to provide quantitative guidelines for prevention.**

Potential Cause of Fall Incidents: Lateral Buckling

Lateral buckling, or lateral torsional buckling, is an instability condition resulting from out of plane movement and twisting of an unbraced or partially braced edgewise beam. Figure 1 demonstrates the beam movement caused by lateral buckling. Lateral buckling is a mechanics phenomenon that can be related to slight eccentricities in load application or initial deflection curvature of the beam. Only edgewise beams, with beam height (h) greater than beam width (b), experience lateral buckling. Note that such beams are typically used as joist and rafter members in residential construction. As the beam is loaded, it remains in plane until a critical buckling moment is reached, at which point the beam commences buckling behavior. Lateral buckling had been defined by various authors including Timoshenko and Gere (1961) and Kirby and Nethercot (1979) for general materials.
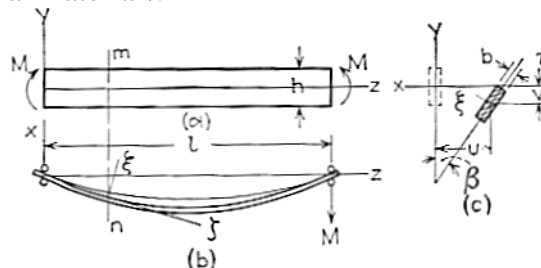

Figure 1: Definition of Lateral Buckling from Timoshenko and Gere (1961)

In terms of falls from elevation, one potential mechanism causing falls from roofs under construction is the lateral buckling of beams. **Typically, the beams give no sign of buckling behavior until the critical buckling load is reached, and then the movement is usually dramatic.** A worker can induce lateral buckling by moving towards the center of the beam, thereby increasing the moment caused by the weight of the worker. The effect of the beam buckling can lead to a loss of balance for a worker standing upon the beam. However, if the beam experiences elastic buckling, once the load has been removed (the worker has fallen), the

beam returns to its undeformed state, showing no damage or change in position. Elastic buckling behavior of solid wood and wood composite beams has been observed by Hindman (2003) in experimental testing.

Lateral Buckling of Solid-Sawn Lumber

Residential construction typically uses solid-wood and wood composite joists in floor and roof construction. Hooley and Madsen (1964) conducted a series of lateral buckling tests upon glued laminated wood beams and developed a relationship for the adjusted bending stress due to lateral buckling concerns. Further refinement of this work (Hooley and Duvall 1964) resulted in the development of three equations to determine the allowable bending stress of wood beams – equations for short beams, intermediate beams, and long beams. It is important to note that the research by Hooley and Madsen (1964) was conducted in 1964. These two research papers (Hooley and Madsen 1964, Hooley and Duvall 1964) were the foundation for the wood design procedures for lateral buckling until the 1992 version of the National Design Specification (NDS) for Wood Construction (AF&PA 2001). Current lateral buckling design in the NDS was developed by Zahn (1992), based on lateral buckling similarities to column buckling behavior which did not include any experimental evaluation, only manipulations of the Hooley and Madsen data.

Lateral Buckling of Wood Composite Materials

Current construction practices for residential structures rely heavily upon solid-sawn lumber products, but have also incorporated a variety of composite wood materials into conventional construction. A family of materials known as structural composite lumber (SCL) is composed of wood strands or plies oriented in the longitudinal direction and bonded by an industrial adhesive. These SCLs are used as alternatives for dimension lumber and have greater strength as well as greater dimensional stability than dimension lumber (Smulski, 1997). Another product widely used in residential construction is the wood composite I-joist. I-joists consist of an SCL flange with an oriented strandboard (OSB) web. These joists come in sizes ranging from 24.1 cm (9.5 in) high to 40.6 cm (16 in) high for residential uses. Figure 2 shows some typical I-joists. Compared to solid-sawn lumber, I-joists are stiffer and stronger, with less weight and less wood fiber used in manufacture. Applications of I-joists include floor and roof joists in repetitive member systems. Over 50% of all new residential construction in the United States uses I-joists (Adair and Camp 2002). I-joists are currently produced commercially by many different companies.

Figure 2: Various types of I-joists

Recent research has studied the lateral buckling of solid wood, SCL, and I-joists. Hindman (2003) and Hindman et al. (2005a and 2005b) measured the lateral buckling loads of a series of solid-sawn lumber, three kinds of SCL including laminated veneer lumber (LVL), parallel strand lumber (PSL), laminated strand lumber (LSL) as well as two different kinds of I-joists. All specimens were subjected to a concentrated load at the free end of a cantilever beam for three different beam lengths to measure the critical buckling load (CBL) to induce lateral buckling. Comparing the CBL values to the load-resistance factor design (LRFD) wood design standard (AF&PA 1996), good agreement was found between the solid-sawn lumber and PSL. The LVL and LSL materials were nonconservatively predicted, while the I-joist values were excessively conservative, indicating that the I-joist lateral buckling capacity is severely underestimated by current design practice. A theoretical model developed by Timoshenko and Gere (1961) that required material property inputs provided a better prediction of experimental values for the I-joists (Hindman 2003).

A further study by Burow (2005) focused on measuring the CBL associated with wood composite I-joists. Both cantilever and center point loading were used to investigate buckling at 22 different lengths ranging from 61 cm to 700 cm (2 ft to 23 ft). The current design model for I-joist strength prediction was found to be overly conservative along the entire range of buckling lengths tested. A moment magnification factor model discussed by Galambos (1998) for steel structures and recently discussed by the American Forest and Paper Association for wooden beams (AF&PA 2003) was applied to model the experimental I-joist data. These methods use a moment magnification factor that relies upon computation of the Euler lateral buckling moment, M_e, which uses the flatwise bending stiffness (EI_y) and torsional rigidity (GJ) of the I-joist.

In residential construction, lateral buckling of wood members, including SCL and I-joists, is only considered a problem during the construction phase of the project. The floor and roof systems are covered with a layer of sheathing and, if applicable, bracing on the underside of the beam. The sheathing negates all concerns of lateral buckling once the construction is finished. However, the process of installing joists and placing temporary bracing and then sheathing materials onto the joists requires workers to traverse the unbraced joists during construction. It should be noted that wood composite I-joist literature warns workers not to walk on unbraced joists (Trus Joist 2001a and 2001b). However, there is no way to enforce this warning or even to ensure that workers know of this danger.

Reported Safety Incidents Involving Lateral Buckling

Many current statistical fatality sources, including the Bureau of Labor Statistics (BLS), present little information upon the cause of many falls from elevation. One additional source that may provide further information as to the likelihood of lateral buckling issues is the Fatality Assessment and Control Evaluations (FACE) conducted by NIOSH. The FACE reports provide background, factual information, and anecdotal recounts of particular incidents. FACE cases which involved falls are compiled in the NIOSH document "Worker Deaths by Falls: A Summary of Surveillance Findings and Investigative Case Reports" (NIOSH 2000). The NIOSH website (http://www.cdc.gov/niosh/face) also provides a link to the directory of FACE reports related to fall incidents. From approximately 375 FACE reports related to falls, the following nine FACE reports show the possibility of an incident caused by lateral buckling.

- FACE 99OH022 May 26, 1999 – A construction laborer fell 30 feet to the ground while installing roof panels. The victim stepped onto an unsecured panel and it gave way, causing the fall incident. Unsecured panels may allow the joists underneath to experience lateral buckling.
- FACE 98CA010 June 29, 1998 – A structural ironworker fell 38 feet from a steel bar joist while attempting to straighten the joist. While bracing one foot on a roof panel, and the other on a joist, the foot on the joist slipped.
- FACE 97MN00801 April 25, 1997 – A worker fell 9 feet into a basement while working on the first-floor joists. The incident was unwitnessed, but occurred while the victim was working on the unbraced floor system. If lateral buckling was the cause of this incident, there would be very little evidence at the site to establish the cause.
- FACE 96NJ05901 August 26, 1996 – An iron worker fell from the roof of a building while attaching steel roof panels when the worker approached the edge of the roof to secure a panel while standing on an adjacent panel.
- FACE 95IN14701 September 13, 1995 – A mechanical engineer fell 22 feet while measuring an opening for HVAC equipment. As the engineer measured the opening, the engineer "stepped onto the tarp covering the metal sheeting and plywood which broke under his weight." This quote seems inconclusive as to whether lateral buckling occurred or the tarp was covering a section of the roof unable to carry the engineer's weight.
- FACE 94CA005 March 10, 1994 – A construction foreman fell 28 feet during roof demolition work. "He was standing on the edge of a panel when the wooden beam supporting the panel shifted." This verbal description from the FACE report strongly indicates lateral buckling caused this incident.
- FACE 93MA012 July 9, 1993 – A metal building assembler fell 33 feet while placing metal decking over the structural steel joists using a roller system. The victim was moving a roller, which slipped from position causing the worker to fall. The roller may have caused the unattached joists to experience lateral buckling because of its weight.
- FACE 88-38 August 11 1988 – A construction foreman was helping to lay insulation over roof panels on a roof with a system of bar joists. As the foreman reached the end of the roof panel, the foreman stepped onto the bar joists, lost balance, and fell to the ground. Lateral buckling of the unbraced bar joists is a possibility because of the loss of balance as a change in material stiffness.
- FACE 88-08 December 7, 1987 – A construction worker was applying a rolled roofing over steel 'Z' purlins. The construction worker stepped onto an unsecured section of metal roofing when "the panel twisted and gave way." Because the roofing was not attached to the Z-purlins at the time of the incident, the roofing was not providing adequate bracing to the Z-purlins which may have experienced lateral buckling causing the worker to loose their balance.

These NIOSH FACE reports center on unfinished structures where the possibility of lateral buckling of unsupported joists may have contributed to the workers' fall incidents. The workers killed in the nine accidents cited above were not wearing or using any kind of fall protection equipment. Of the 375 FACE reports for falls examined, these nine were considered to be caused by lateral buckling. Thus, 2.4% of the fall incidents reported by NIOSH FACE reports contain some lateral buckling. Extrapolating this percentage to the number of worker fatalities from falls in the construction industry in 2004 (815) (BLS 2004a), lateral buckling may be responsible for 19 falls per year. Using the figures from Lipscomb et al. (2003a), these 19 falls caused by lateral buckling cost the construction industry an average of $330,000 per year. These

reports only encompass studied fatalities and do not account for workplace injuries, however severe.

Recent Research Modeling the Loads Imposed by Walking

Another needed component to complete this research is the behavior of unbraced beams due to workers walking or other loads caused by specific construction worker tasks upon the lateral buckling characteristics of the I-joists. The loads induced by walking are not considered static, but involves two distinct load peaks caused by the heel and toe contact of each foot (Tirosh and Sparrow 2003). Walking also has a decided lateral component of medio-lateral stabilization involved in foot placement Donelan et al. (2004). This introduction of a lateral load component can induce a twisting moment in the beam, causing lateral buckling to occur at lower load levels than the case of only vertical loads. Obata et al. (2006) modeled the force response over time of a person walking using the load-time curve shown in Figure 3 for understanding the dynamic behavior of a pedestrian bridge. The force axis is normalized to a person's weight (100% of weight = 1). Note that in Figure 3, during the heel and toe contacts, the force applied to the structure is greater than the weight of the person.
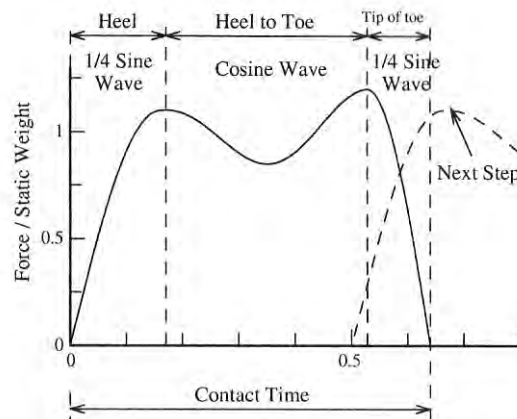

Figure 3: Model of the Force Applied Over Time for a Single Step[38]

Preliminary Study

Recently, Dr. Hindman received funding from the Center for Innovation in Construction Safety and Health, a NIOSH-funded center at Virginia Tech, to conduct an initial set of lateral buckling measurements in support of this research proposal. This work focused on the test method development to measure the lateral buckling load of long-span I-joist beams. Conditions explored included both static loading and dynamic loading caused by walking. Two different kinds of I-joists, a TJI 230 30.2 cm (11-7/8 in) tall and a TJI 360 35.6 cm (16 in) tall product from Trus Joist, a Weyerhaeuser company, were used for evaluation (Trus Joist 2005). Nine samples of each I-joist were tested.

The static loading configuration included a simply-supported beam with a clear span of 19 feet and a point load applied at the center of the span. This arrangement should produce the worst case buckling load. Loading was applied using an MTS universal testing machine with a loading rate of 0.25 inch/min. Figure 4 shows the fixture for measurement of lateral buckling. This fixture applies the load to the tension flange of the I-joist, while allowing the entire I-joist to pivot about the hinge located at the bottom of the fixture. Figure 4b shows the I-joist being tested using the fixture from Figure 4a. This work demonstrates that the lateral buckling load due to an unbraced static load can be measured.

(a)   **(b)**

Figure 4: Static Loading of I-joists, (a) Loading Fixture, (b) I-joist Undergoing Buckling

Table 1 shows the mean and coefficient of variation (COV) values from the two types of I-joists tested. These I-joists were manufactured by Trus Joist, a Weyerhaeuser business (Trus Joist 2005). The TJI 230 I-joists had a height of 30.2 cm (11-7/8 in) and a flange width of 5.9 cm (2.3 in), while the TJI 360 I-joists had a height of 35.6 cm (14 in) and a flange width of 5.9 cm (2.3 in). The buckling load increased with increasing size of the I-joist, which is expected due to the increased bending stiffness of taller sections. The COV of the buckling load is about 10%, which is currently assumed for wood composites (USDA 1999). If the average weight of a construction worker is considered at 250 lbs (including tools), the TJI 230 I-joists will experience buckling well before the worker gets to the midspan of the beam. Considering the variability of the material, there is a chance that the average weight of a construction worker may cause buckling of the TJI 360 I-joists at or near the midspan of the beam. Again, this section of the research only considers the static load of a worker.

Table 1: Buckling Loads from I-joists Determined From Static Loading

I-joist	Mean Buckling Load	COV
TJI 230	183	9.4%
TJI 360	262	10.8%

To measure the force due to walking, load cells were placed under the supports of the unbraced beam to measure the force applied by a walking load. The subject shown in Figure 5a weighs approximately 200 lbs and conducted the experiments using the two I-joists described earlier. The force that the worker transmits to one support will vary as the beam is traversed. Figure 5b shows the load-time measurement from one support with the subject walking towards the center of the I-joist. This load-time graph is a composite of several safety platform positions to describe the subject walking from one end to the center of the beam. As the subject nears the middle of the beam, walking becomes difficult as the beam starts to buckle. The noise in the load-distance curve at the right side of Figure 5b shows the change in load caused by lateral buckling.
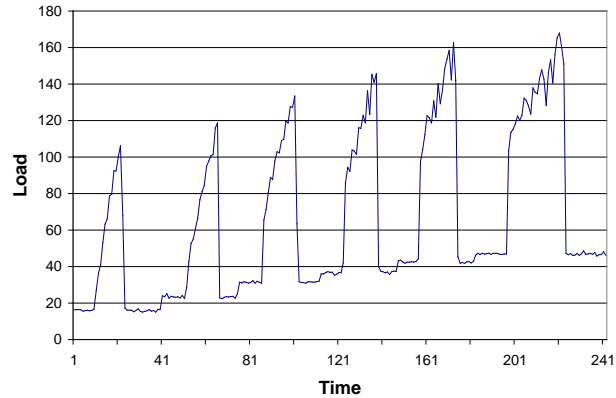
Figure 5: (a) Subject Walking on I-joist (instructed to exert minimal forces on the safety rail); (b) Load Measured at End Support

This preliminary work lays the foundation for this research proposal to investigate the lateral buckling of unbraced wood composite I-joists. Test methods for the measurement of static and dynamic loadings of unbraced beams have been demonstrated. These techniques can measure the static buckling loads of a beam undergoing buckling. Also, the dynamic components associated with walking loads were significant compared to the static loading, especially as the beam nears the lateral buckling moment, so that the dynamic forces must be considered.

Conclusion of Background

The problem of falls from elevation on construction sites is very serious, taking a toll in deaths, injuries, and additional costs. Current research efforts on fall prevention have investigated the demographics of fall victims, but little work has been completed that examines the contribution made to falls by the mechanics of materials used in the structure. One area of construction that has not received much attention is falls from elevation on residential construction sites, which use wood and wood composite materials for construction. One possible cause of falls from unbraced joists during construction is lateral buckling. **Fall incidents caused by lateral buckling are entirely preventable.** Currently, for wood beams, especially SCL and I-joists, there is little understanding of the loads or unbraced lengths where lateral buckling will occur. In fact, the five studies cited here (Hindman 2003, Hindman et al. 2005a and 2005b, Burow (2005) and Zhu (2005)) are the only known published studies on the lateral buckling of I-joists. However, wood composite I-joists are manufactured by a variety of companies in a large range of sizes and flange thicknesses, which have not been studied in an extensive manner.

Specific Aims

The goal of this research is to explore the relationship between construction worker loadings and mechanical behavior causing lateral buckling of wood composite I-joists. Specific aims are to characterize the loading caused by workers performing tasks upon unbraced beams, to model the lateral buckling behavior of wood composite I-joists, and to suggest possible methods for preventing falls as a result of lateral buckling. This research is novel in the study of a particular cause of falls and in the study of lateral buckling of wood composite I-joists, which is not a well understood phenomenon. Results of this research will serve as an initial step toward the development of design and usage guidelines to prevent falls resulting from lateral buckling.

15

Specific Aim #1. Characterize the static and dynamic loading caused by construction activities on unbraced beams. Construction site observations will provide initial data on the actions of workers. These loads caused by these construction activities will then be measured using laboratory instrumentation. This specific aim is an exploratory component to provide information for Specific Aim #2.

Specific Aim #2. Model and verify the lateral buckling behavior of unbraced wood composite I-joists. Models used will include the theoretical definition of lateral buckling, current solid-wood design criteria, and proposed wood composite design criteria. Verification of models will use testing of unbraced wood composite I-joists subjected to the loadings measured in Specific Aim #1.
Primary Hypotheses:
1. Model results from the current wood design criteria for lateral buckling of I-joists will be less than experimental results.
2. Model results using a finite element analysis and a moment magnification factor will provide good agreement with the experimental results.

Specific Aim #3. Formulate prevention strategies to limit lateral buckling hazards based upon the results of Specific Aims #1 and #2. Concepts of reliability will be used to compute a buckling length which workers could traverse with little possibility of lateral buckling occurring. Other strategies to warn workers of the danger of lateral buckling will be examined.

Methodology
Materials
Test specimens consisted of three different sizes and lengths of wood composite I-joists from two manufacturers; Georgia Pacific and iLevel, a division of Weyerhauser (formerly know as TJI). These joists represent the most common sizes used in residential construction. The Georgia Pacific I-joists had overall heights of 11 7/8" and 14", referred to as GP12 and GP14, respectively. The TJI joist manufactured by iLevel had an overall height of 11 7/8" and was referred to as TJI12. Table 2 shows typical dimensions of the I-joists and the ICC Evaluation Service report numbers. While the specimens were not conditioned to any specific moisture content, the I-joists were allowed to acclimate to the testing environment of approximately 10% equilibrium moisture content (EMC) in the Wood Engineering Laboratory at the Brooks Forest Products Center.

Table 2. Product Names and Dimensions of Wood Composite I-joists Used in Study

Product Name	ICC-ES Report	Overall Depth	Flange Width	Web Thickness
GP 12	ESR- 1325	11-7/8"	2-7/16"	3/8"
TJI 12	ESR- 1153	11-7/8"	2-5/16"	3/8"
GP-14	ESR-1325	14"	2-7/16"	3/8"
GP 16	ESR- 1325	16"	2-7/16"	3/8"

Specific Aim #1
This specific aim combined jobsite observation with laboratory analysis to quantify the load capacity workers placed upon unbraced beams during typical construction activities. First,

characterization of construction worker activities on unbraced beams was obtained from jobsite observations. Both static and dynamic loading of the I-joists were conducted. Static loading used a single point load at the center of the beam. Dynamic loading used an improved safety platform where the support loads as well as joist displacements at discrete points along the joist were measured. These loads were then be used in Specific Aim #2 to verify the lateral buckling models.

Jobsite Observations
Observations of several jobsites in the area surrounding Blacksburg, Virginia were conducted. Visits were made to two roofing sites at two unannounced times to observe workers on unbraced floors. Most of the situations observed were roofing placement of sheathing. Permission was obtained from the contractors before and no contact was made with the workers to prevent any bias.
At the conclusions of observations, the researchers reviewed the video and pictures. This information was used to help guide laboratory measurements of joist movement due to worker loads. No statistics were applied due to the small number of observations made.

Static Test Procedure
Static testing of wood composite I-joists was conducted to understand the load-displacement behavior. Static testing requires little specialized equipment compared to dynamic testing. Figure 6 shows the test method used for static loading. The joists were simply supported with the load applied in the center. Table 3 shows the number specimens of each joist used for static testing. These numbers of I-joists were relatively low compared to wood material testing due to previously measured performance. Six loading repetitions of each joist were conducted to examine the variability of loading method. All static testing was conducted with a servo-hydraulic Material Testing System (MTS) utilizing a MTS 661.20E-01 5000 lb load cell with an error of less than 1 percent. Data was collected through the use of National Instruments LabVIEW 7.0.

Figure 6. Static Testing of I-Joists Using Center Point Load

Table 3. Static and Dynamic Testing Parameters of I-joists

Joist	Static Loading			Dynamic Loading
	Length of Joist, ft	Load Rate, in/min	Maximum Load, lb	Length of Joist, ft
GP 12	20	0.10	500	20
TJI 12	24	0.16	500	24
GP 14	20	0.07	400	20

Lateral displacements of the top and bottom flanges as well as the rotation of the beam were recorded at the midpoint and quarter point. UniMeasure PA-5-L3M and PA-2-L3M string potentiometers, with an error of less than 1 percent of the measured values, were attached to the beam at the midspan and quarter point of the top and bottom flange, as illustrated in Figure 7, to measure the lateral deflection. The 5 inch potentiometers were placed at the midspan of the joist to allow for the possibility of exceeding the 1 inch lateral movement of a 2 inch potentiometer. The other potentiometers were placed at the quarter point. The rotation was recorded through the use of AccuStar 11/DAS 20 clinometers, with an error of less than 1 percent, clamped at the midpoint and quarter point of the bottom flange.
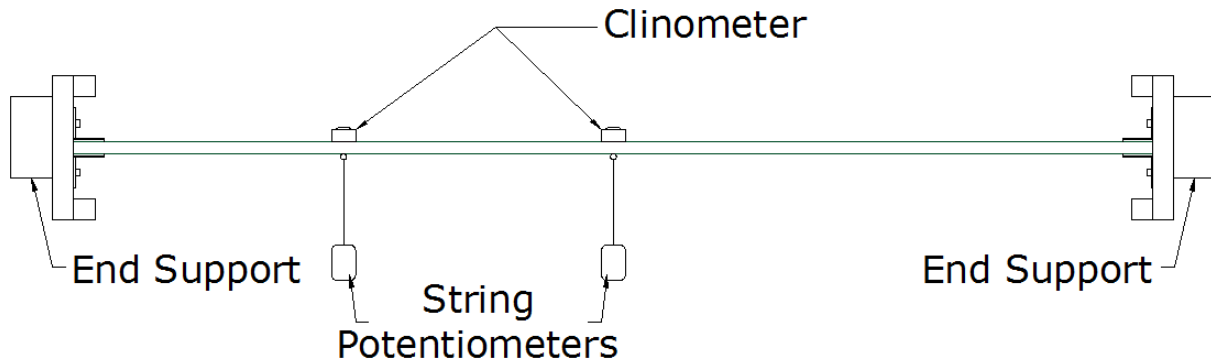

Figure 7. Plan View of Measurement Devices Used in Static Bending Test

String potentiometers were attached to the testing machine and restrained from moving as the joist deflected. Since the downward deflection of the hydraulic ram of the MTS testing machine was not measured, the lateral displacement measurements included some effect from the vertical displacement. The potentiometers were mounted approximately 8 inches from the joist to minimize the angle occurring at the maximum vertical deflection. To ensure that the downward deflection was not a significant influence on the lateral displacement, initial test conducted using linear variable differential transformer (LVDT) placed at the midpoint of the top flange of the I-joist to measure lateral displacement. Differences between the readings of the string potentiometer and the LVDT were attributed to the vertical deflection. These tests indicated that the string potentiometers were sufficiently distanced from the test specimen so that the downward deflection was not significant and found to be less than a change of 0.015 inches.

A special end support was constructed using an appropriately sized joist hanger to replicate field conditions. The end supports, shown in Figure 8, were constructed from LVL and placed atop a steel post to elevate the I-joist above the bed of the testing machine. Each joist was placed within the joist hangers and shimmed tight at the top and bottom flange. This prevented any global displacement of the joist - lateral or rotational - from occurring.

18

Figure 8. End Support with Joist Hanger

The use of a standard load head acts as a lateral and rotational bracing point inducing a higher order buckling mode. To account for this, a specialized roller bearing plate was placed under the load cell of the MTS machine. The roller bearing plate, shown in Figure 9, consisted of four rows of five linear bearings underneath a metal plate. This load head allowed the joist to move laterally and rotate slightly in either direction allowing only vertical forces to load the joist. The specialized bearing plate combined with the swivel head allowed the joist to move freely within the test range.

Figure 9. Bearing Support and Swivel Head

To begin each test, each joist was placed into the joist hanger on the end supports. Care was taken to make sure the joist was then directly centered underneath the load cell. Shims were installed between the top and bottom flanges of the joist and the joist hanger. Sufficient force was applied to the shims to prevent the joist from moving from side to side within the joist hanger. Metal eye hooks were installed in the center of the top and bottom flanges at the midpoint and quarter point to receive the string potentiometers. The potentiometers were connected to the I-joist using brass wire with the length of wire adjusted so that each potentiometer was centered with respect to its sensor range. The roller bearing plate was then clamped to the center of the joist on the top flange and leveled by adjusting the tension of the clamps.

The MTS machine applied a constant deflection rate depending on the type of joist being tested. Table 2 shows the loading rates used for the static test; the loading rates were calculated to reach a 500 lb load in 5 min. The GP12 and GP14 joists were loaded to 500 lb. Due to the increased length, the TJI12 joists were loaded to 400 lb.

The data collected consisted of four deflection readings and two rotation measurements. The raw data was processed through the use of MATLAB R2008b. MATLAB was used to automate the process of reducing the data to a series of load-deflection and load-rotation graphs. The starting point of the test was adjusted to the time at which load was starting to be applied and the end point was taken at 500lb. The data was then stored into an Excel file for further manipulation. The statistical analysis focused solely on linear regressions of the load-deflection and load-rotation plots. The slopes of each regression were compiled and analyzed with JMP 7.0.1. The data was first analyzed using a two factor ANOVA test, with a significance level of $p < 0.05$. The independent variables, joist and replication, were modeled as random effects. After confirming that there was no significant difference between the replications, the data was reanalyzed without the replication factor.

Dynamic Test Procedures

The second objective of this research was to record the induced loads and deflections of a construction worker traversing the joists. Figure 10 shows the improved safety platform used for all dynamic testing. The safety platform consisted of two portal frames connected with a truss-like safety rail on either side. A steel beam, to which test subjects would be tethered, was install spanning between the two portal frames.
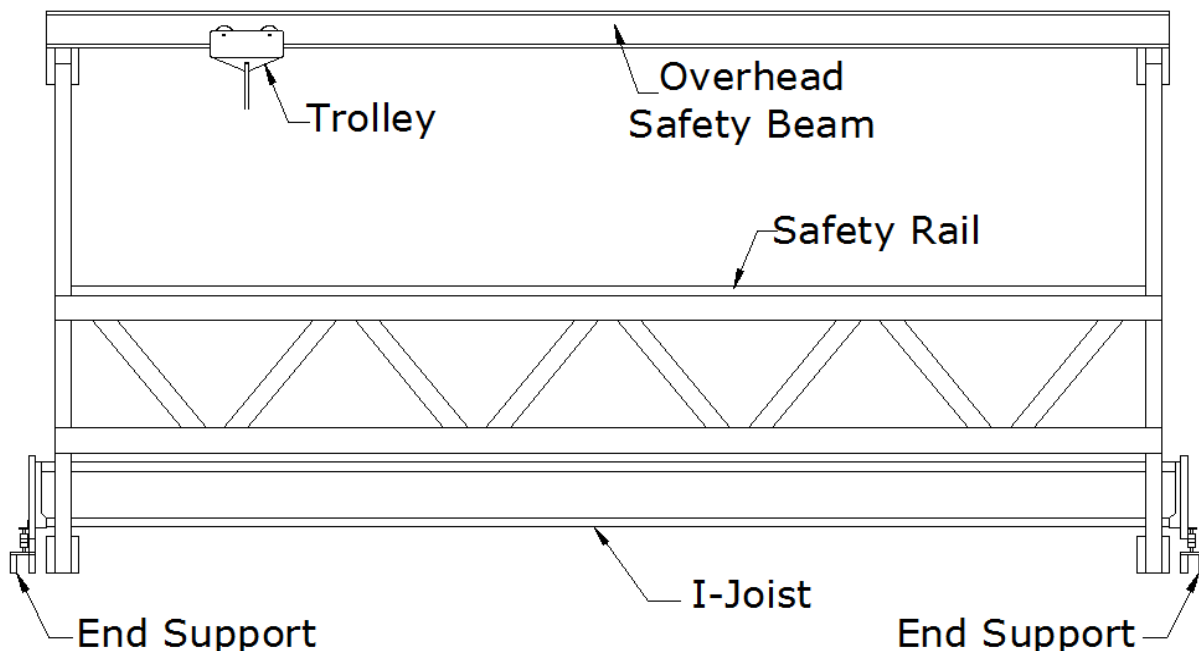

Figure 10. Side View of Safety Platform

Two different end supports were constructed to hold the ends of the I-joist and the four load cells necessary to capture the induced loads. Vishay BHL U3SB-A "S" type load cells with

a 5000 lb capacity and an error of less than 1 percent were be placed at both ends of the beam to record the end reactions and allow for calculating the test subject's position on the beam. One one support, load cells were also attached in the vertical direction and at the top and bottom flanges. On the other support, a single load cell was mounted in the vertical direction. All load cells were attached to an LVL section with an attached joist hanger. Figure 11 shows the two end supports used. The vertical load cells were used to calculate the test subjects' position along the beam. The end reactions combined with the I-joist flange reactions were then compiled resulting in a combination of loads and movement the test subject applied to the I-joist.

(a)   **(b)**

Figure 11. (a) End Support with 3 Load Cells (b) End Support with 1 Load Cell

       A pair of 20 inch long string potentiometers, UniMeasure model PA-20-L3M, were placed at the mid-span and quarter-span, as shown in Figure 12. At each location, potentiometers were attached to the top and bottom flange. Unlike the static test, the use of clinometers to measure the rotation of the beam was not possible due to the rapid movement of the I-joist producing inaccurate and muted results. Instead, the rotation was calculated by trigonometry from the string potentiometers connected to the top and bottom flanges. This calculation assumed that the web of the joist remained perpendicular to the flanges. All data from the load cells and potentiometers was collected using a Vishay Micro-Measurements StrainSmart 4.31 data acquisition system.
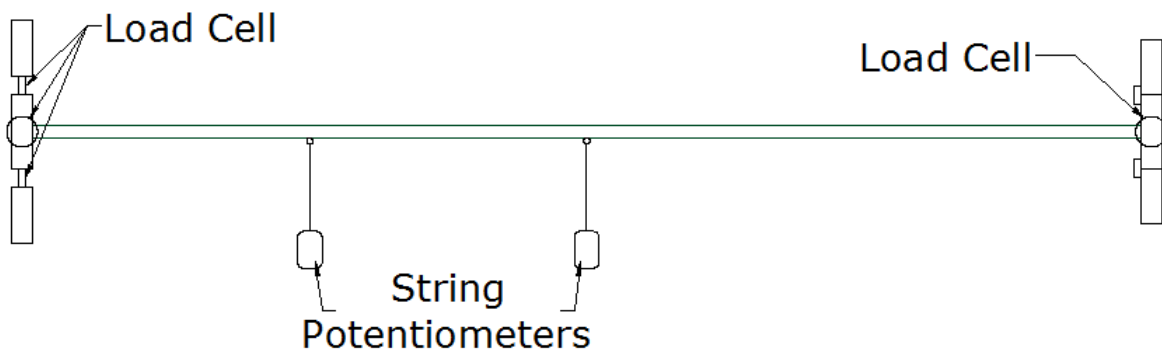

Figure 12. Plan View of Measuring Devices along I-Joist for Dynamic Testing

Test subjects consisted of Caucasian, Hispanic, or Indian males who were construction workers or graduate students. The weight of the test subjects ranged from 133 lbs. to 283 lbs. All data collected from test subjects conformed to the Virginia Tech Internal Review Board. To begin each test, the subject's weight was recorded on an Arlyn Scale Model 320m. An I-joist was then placed between the end supports. The flanges of the I-joist were shimmed against the joist hangers to prevent lateral movement. A test subject, wearing a construction safety harness, was tethered to the trolley that rides along the overhead safety beam. Each subject traversed the beam two times at a comfortable walking speed for the test subject. The test subject were allowed to walk at their own pace, but were instructed to maintain a constant speed. The test subjects were further instructed to use the safety rails only when necessary to prevent a fall. Use of the safety rails would invalidate that test data since load would be transferred away from the I-joist under study. Figure 13 shows a test subject traversing one of the I-joists.
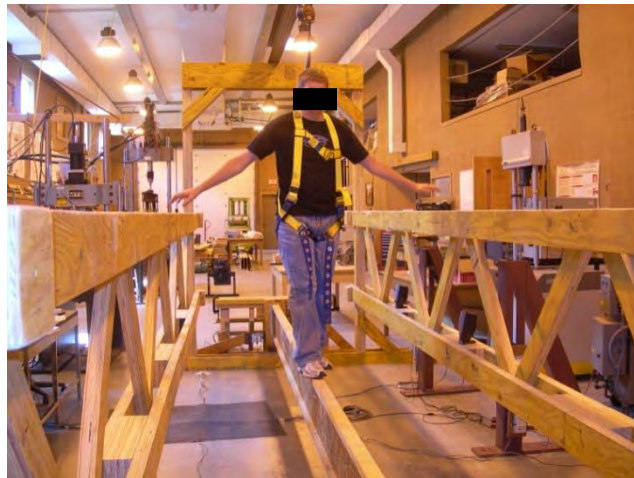

Figure 13. Test Subject Traversing I-joist

Specific Aim #2

The purpose of this specific aim is to model the lateral buckling behavior of a variety of different wood composite I-joists considering static and walking loads measured from Specific Aim #1. Several models to describe the lateral buckling behavior were developed. These models included a finite element model (FEM), and theoretical equations from mechanics of materials. Material properties associated with each type of I-joist were evaluated for model inputs. Model predictions were compared to experimental lateral buckling results (Specific Aim #1) for validation.

Finite Element Model Construction

A finite element (FE) analysis of each type of I-joist was conducted with ANSYS version 11. FE models were developed utilizing the available properties of the laminated veneer lumber (LVL) and oriented strandboard (OSB), summarized in Table 4, to represent the behavior of each wood composite I-joist. LVL and OSB materials were modeled as orthotropic materials with axis alignment described in Figure 14. The mechanical properties used in the FE models were derived from previous research by Janowiak et al. (2001), the Wood Handbook (USDA 1999), as well as manufacturer specifications (Weyerhaeuser 2004). The modulus of elasticity, E, in the X and Y directions as well as the three shear moduli were determined according to the average

southern yellow pine values reported by Janowiak et al. (2001). The LVL Poisson's ratio was the same value as loblolly pine from the Wood Handbook (USDA 1999). The E in the X and Y directions for the OSB web were determined from the manufacturer's specification (Weyerhaeuser 2004). Poisson's ratios and shear moduli for the OSB were considered equal to loblolly pine from the Wood Handbook (USDA 1999). Although from different manufacturers, all three joist types were assumed to have identical mechanical properties.

Table 4. Mechanical Properties of OSB and LVL

LVL		OSB	
E_X	8.94E+04	E_X	2.09E+05
E_Y	8.94E+04	E_Y	1.14E+06
E_Z	2.38E+06	E_Z	2.09E+05
ν_{XY}	0.382	ν_{XY}	0.054
ν_{YZ}	0.011	ν_{YZ}	0.328
ν_{XZ}	0.012	ν_{XZ}	0.362
G_{XY}	9.64E+03	G_{XY}	9.22E+04
G_{YZ}	5.14E+04	G_{YZ}	9.33E+04
G_{XZ}	6.57E+04	G_{XZ}	1.48E+04
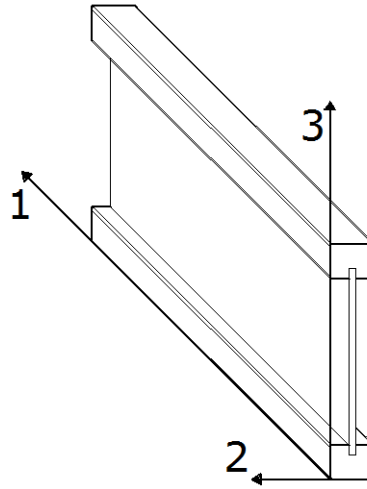
Figure 14. Coordinate Axes Orientation for Composite Wood I-Joist

The FE models were comprised of 10 node solid brick elements shown in Figure 15(a). End conditions and loading points are shown in Figure 15(b), while a cross sectional view of the FE mesh is shown in Figure 15(c). Three rows of hardpoints were created along the top and bottom flange. Hardpoints were used to map a known value to a corresponding node generated by the meshing process. The hardpoints were located on the outer surface of the model and were used to control the application of load and interpret the displacement results. A single row of hardoints, spaced one inch apart along the center of the top flange surface, allowed the placement of the test subject's static weight. Hardpoints spaced one inch apart along the side of the top and bottom flanges allowed for placement of the test subject lateral loads.
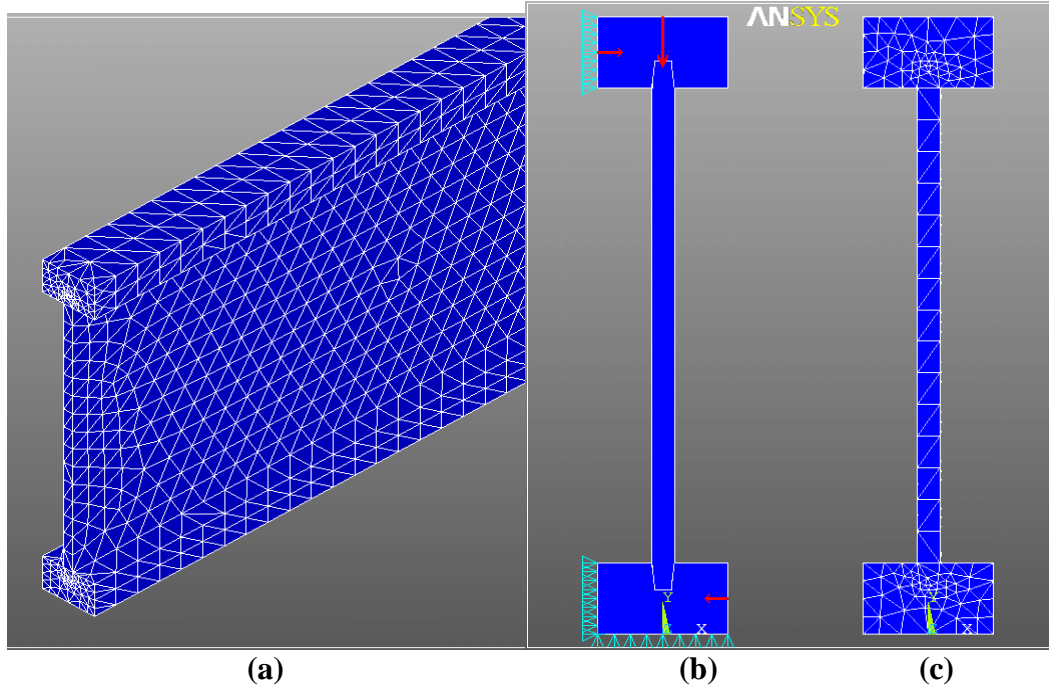
(a)   **(b)**   **(c)**
Figure 15. (a) 3D Model (b) Boundary/Loading Conditions and (c) FE Mesh

The FE mesh was applied to each solid model through a free mapping process using tetrahedral shaped elements. The spacing of elements in the FE mesh was controlled by the placement of the hardpoints. The amount of refinement required to avoid an abundance of mesh incongruities in the FE mesh was well beyond that which would have been required by a detailed convergence study. A convergence study of two iterations was performed on a single model by decreasing the distance between hardpoints by a factor of two. The model was loaded statically at the midpoint. The convergence study found a less than three percent difference at midpoint, indicating that the level of refinement was appropriate. No refinement between hardpoints was necessary. Since only displacements were monitored in this research, less refinement of the model was required than models calculating stresses and strains.

The end boundary conditions of the FE model closely reflected conditions found in the field during joist installation. The bottom flanges of the joist were fully supported along the outer surface against deflections in the plane of the web. The top and bottom flanges were restrained against lateral deflections on one side. Since the joist hangers used to install these beams lack sufficient rotational stiffness, only one side was braced against lateral deflection, allowing the ends of the joist to rotate slightly. Only one node was restrained against deflections along the longitudinal axis of the joist to avoid instability problems when solving the model.

Finite Element Model Analysis

The models were subjected to two analyses with different loading conditions. Both analyses were conducted as transient dynamic analyses without consideration for vibration, dampening, or any harmonic effects. Each analysis was treated as a series of load steps, with each load step capable of analyzing a given set of loading conditions at different points. This analysis also imposed the previous load step's deformations on the current load step before solving the analysis.

25

First a full pseudo-dynamic analysis was conducted using a point-by-point basis on the FE model. Lateral loads were applied to the model at respective hardpoints according to the top and bottom flange load cell readings recorded in Specific Aim #1 dynamic loading adjusted for the placement of the load along the length of the joist. Simultaneously, the corresponding static weight of the test subject was applied as a vertical force to the corresponding hardpoint at the center of the top flange. The time index of this analysis was controlled by the time index of the lateral loads taken from Specific Aim #1 dynamic loading. Due to the complexity and length of time required to solve a full analysis, only three of the test subjects were modeled per joist type. For statistical purposes, both of the tests subject's attempts to traverse the three joists of each joist type were modeled.

A second FE analysis was conducted to generalize the results of dynamic loading. This analysis used the maximum applied lateral load on the top flange and the average applied load on the bottom flange from dynamic loading. The average value applied to the bottom flange compensated for the fact that the peak load for both flanges did not occur at the same time. The values were obtained from each test conducted and normalized to a percentage of the test subject's static weight. The two lateral loads at the top and bottom flanges were applied in opposite directions to simulate torsion in the I-joist, while the static weight of the test subject was applied to the top flange. All three forces were applied at 24 evenly spaced points along the length of the member to produce the outer displacement bounds of the I-joist. This analysis was performed for each combination of test subject and I-joist type.

ANSYS model outputs consisted of only nodal displacements. As in the physical testing of the beams, the angular rotation was extracted from the lateral displacements generated by ANSYS. The rotation was computed from the difference in the top and bottom flanges at the hardpoints corresponding to the midpoint and quarter point of the joist, which could be directly compared the lateral displacement and twist measurements from Specific Aim #1. Since the hardpoints were located on opposite sides of the beam, the cross section was assumed to remain planar. The lateral displacements and angular rotations at the mid-span and quarter-points were analyzed and compared to the dynamic loading.

Validation of Finite Element Model

Two difference analytical procedures were created - one for the input into the full pseudo-dynamic analysis and the other for a simulated pseudo-dynamic analysis. For both procedures, loading data was condensed using MatLAB and Excel based on the starting and stopping of the tests. The starting point was when the test subject transferred a significant amount of their body weight, approximately 75 lbs, onto the joist. The stopping point was when the amount of load remaining on the joist was 75 lbs. The lateral load data from the top and bottom flange was adjusted based on the position of the test subject assuming a linear relationship between time and walking speed. This data was inputted into the full pseudo-dynamic and the simplified models to produce nodal displacements.

Statistical comparisons analyzed the similarity of the applied static loads and dynamic loading from the test subjects. The lateral deflection and twist of the dynamic tests were compared to deflections generated by the finite element model. Because statistical comparisons of the model output and test results were difficult, only the outer bounds of each test and simulation were compared. This allowed the model and test data to vary slightly with time, without a significant detriment to the model's validity. To capture the outer bounds of both the

ANSYS generated data and the loading data, the absolute value of each deflection and rotation was taken, forming an absolute value curve.

The maximum value of each test was then determined. The maximum value was used as a dividing point for the graph, creating the maximum value curve (MVC). Figure 16 illustrates the development of the MVC from the raw data in Figure 16(a). Taking only increasing data points from both the start and the end of the absolute value curve creates the maximum value curve seen in Figure 16(b). This curve represents the outer bounds that the joist traveled during the test.
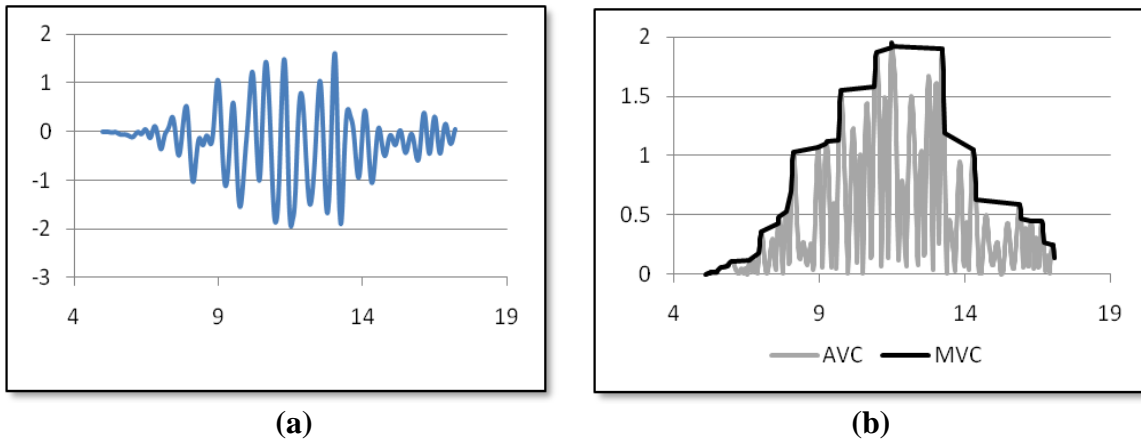

(a)   (b)

Figure 16. (a) Acquired Test Data (b) Absolute Value Curve and Maximum Value Curve

The MVC for each deflection and rotation generated from the acquired data was matched to the corresponding MVC from the ANSYS model. The difference between the MVCs was calculated and considered to be the amount of error in the model. A running average of the model error was calculated and used to determine at what distance from the start of walking the model deviated significantly from the test data. When the error exceeded 10 percent of the maximum value acquired from the experimental MVC, the model was said to no longer be effective. Since the effects of vibration and dampening were not accounted for in the model, error values under 10% maximum value were considered acceptable.

Theoretical Models

Lateral buckling instability is influenced by the end support conditions, loading conditions as well as bracing systems (Kirby and Nethercot 1979). Three different end support conditions were analyzed in this model: simply supported, fixed and hanger fixed. The hanger fixed end condition was modeled using a lateral spring analogy. Differences between hangers were incorporated into the model by the lateral spring stiffness term. Two different lateral buckling models were developed for each of the three end support conditions, a static lateral buckling model, and a pseudo-dynamic lateral buckling model.

The static lateral buckling models were developed using the strain energy method. The pseudo-dynamic lateral buckling models were developed by linearly combining the static lateral buckling models with the lateral bending motion of the wood I-joists. The bending motion of the wood I-joists was analyzed using the lateral component of the force imposed by a test subject walking on the wood I-joists and an adjusting function to simulate the average variation of the response of the wood I-joists to the test subject's walking. A different adjusting function was proposed for each of the three end support conditions. Three bracing systems were analyzed for

each of the three end support conditions as well as for the two lateral buckling models: no-bracing, one mid-span brace, and two quarter-span braces. Equations for the amount of bracing restraint due to the bracing system were derived for the one mid-span brace and two quarter-span braces.

Equations were derived based on the differential equations of equilibrium method as well as the strain energy method using the end support conditions as boundary conditions. In the strain energy method, the function β for the angle of twist must satisfy the end support conditions. Poor end fixity creates smaller critical lateral buckling loads while strong end fixity configurations create larger critical lateral buckling loads (Timoshenko and Gere 1961). Three different end support conditions were used in this research to describe the lateral buckling instability in wood I-joists. The three end support conditions were simply supported, fixed, and hanger fixed.

In the simply supported end condition, the ends of the joist can rotate freely with respect to the principal axes of inertia parallel to the x-axis and y-axis, while rotation about the z-axis is prevented. A simply supported end condition is most commonly used in literature since this condition is assumed for most typical connections (Kirby and Nethercot 1979). When the simply supported end condition is not used in practice adjusting factors can be applied to modify the simply supported end condition to other end support conditions (AF&PA 2003). In research, the simply supported end condition is considered the basic case. More complicated end support conditions are often compared to the simply supported end condition (Kirby and Nethercot 1979). Figure 17 depicts the simply supported end condition.
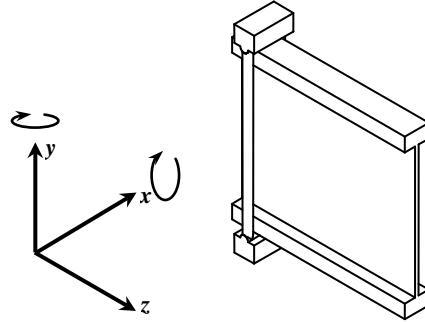

Figure 17. Simply Supported End Condition

In the simply supported end condition, the wood I-joist flanges are supported at the bottom and laterally by round bars that allow rotation. The wood I-joist web is not supported and is assumed to undergo zero lateral displacement. Displacements and moments at the ends for the x-axis and y-axis are equals zero. Mathematically the simply supported end conditions are expressed by the following equations.

$$x(z,t)=0 \quad and \quad \frac{\partial^2 x(z,t)}{\partial z^2}=0 \quad for \quad z=0 \quad and \quad z=l \tag{1a}$$

$$y(z,t)=0 \quad and \quad \frac{\partial^2 y(z,t)}{\partial z^2}=0 \quad for \quad z=0 \quad and \quad z=l \tag{1b}$$

A fixed end support condition has no rotation at the ends of the wood I-joist in any direction. This condition is the strongest end fixity that can be reached in theoretical analysis

and practical circumstances. A fixed end support condition is difficult to develop in residential construction for wood I-joists. However, this end support condition can be approximated in practice when strong end fixity hangers are used. Hindman et al. (2005b) applied a dead load to a wood I-joist specimen and approximately reproduced a 96% end support condition according to mechanics equations. Figure 18 depicts the fixed end support condition.
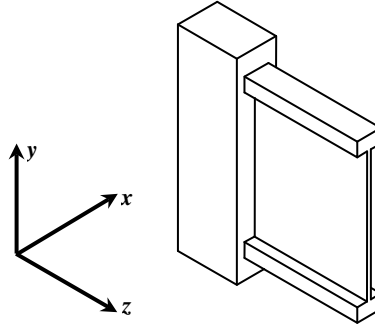

Figure 18. Fixed End Support Condition

In the fixed end support condition, displacements and deflections at the ends for the *x*-axis and *y*-axis equal zero. The wood I-joist web is fully supported and is assumed to undergo zero displacement and deflection. Mathematically the fixed end supported conditions are expressed by the following equations.

$$x(z,t)=0 \quad and \quad \frac{\partial x(z,t)}{\partial z}=0 \quad for \quad z=0 \quad and \quad z=l \tag{2a}$$

$$y(z,t)=0 \quad and \quad \frac{\partial y(z,t)}{\partial z}=0 \quad for \quad z=0 \quad and \quad z=l \tag{2b}$$

The hanger fixed end support condition is a model of real end support conditions found in practice in the residential construction industry when wood I-joist hangers are used. Hanger fixed end support condition allows the ends to rotate freely with respect to the principal axis of inertia parallel in the *x*-axis and *y*-axis directions. Lateral displacements at the ends are restored by springs in the principal axis of inertia parallel in the *y*-axis direction, while rotation in the *z*-axis is prevented. Figure 18 depicts a physical model of the hanger fixed end support condition. The model uses a spring support with a stiffness constant *k* in the lateral direction. The axial support was assumed to be the same as the simply supported end condition. Differences between end fixity from several wood I-joist hangers were incorporated into the model by adjusting the spring stiffness constant, *k*.
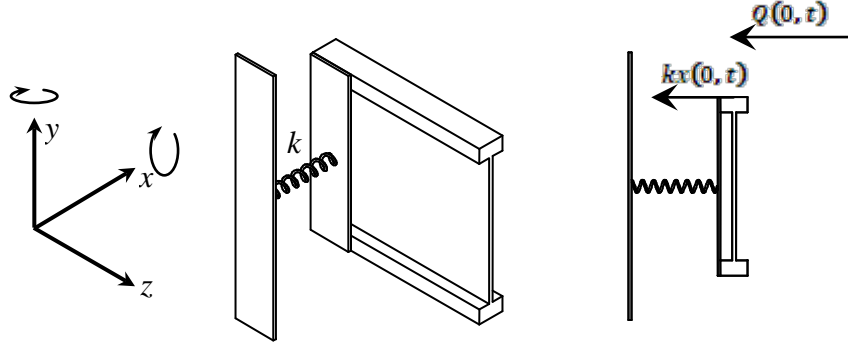
Figure 19. Model of a Hanger Fixed End Support Condition

The reaction force in the spring is $kx(0, t)$. This reaction equals the shear force in the wood I-joist. Assuming that the lateral bending stiffness EI_y has a constant value throughout the wood I-joist, the shear force can be expressed with the following equation.

$$Q(z, t) = -EI_y \frac{\partial^3 x(z, t)}{\partial z^3} = kx(z, t) \tag{3}$$

In the hanger fixed end support condition, displacement in the axial direction and moments at the ends equal zero. Mathematically, the hanger fixed end supported condition is expressed by the following equations.

$$-EI_y \frac{\partial^3 x(z, t)}{\partial z^3} = kx(z, t) \quad and \quad \frac{\partial^2 x(z, t)}{\partial z^2} = 0 \quad for \quad z = 0$$

$$-EI_y \frac{\partial^3 x(z, t)}{\partial z^3} = -kx(z, t) \quad and \quad \frac{\partial^2 x(z, t)}{\partial z^2} = 0 \quad for \quad z = l \tag{4a}$$

$$y(z, t) = 0 \quad and \quad \frac{\partial^2 y(z, t)}{\partial z^2} = 0 \quad for \quad z = 0 \quad and \quad z = l \tag{4b}$$

Static Lateral Buckling Model

Static loading refers to an applied load at a single point gradually increasing until lateral buckling instability occurs. The static lateral buckling models were developed using the strain energy method. These models were then used to develop the pseudo-dynamic lateral buckling models. Assumptions include the loading was applied at the top flange of the wood I-joist, and small changes of energy from axial deflections was neglected. The function β for the angle of twist for a simply supported wood I-joist was described by Timoshenko (1936).

$$\beta = \sum_{n=1}^{\infty} b_{(2n-1)} \cos\left(\frac{(2n-1)\pi z}{l}\right) \tag{5}$$

The best approximation for the static critical lateral buckling load was obtained by adjusting the variables b_1, b_2, b_3…, to minimize Equation 5. By using a single term in Equation 5, the accuracy of the solution was suitable for practical applications (Timoshenko 1936).

Considering that the load is applied at the mid-span ($s = \frac{l}{2}$) and using a single term for β from Equation 5, the following equation for the static critical lateral buckling load was obtained for a simply supported wood I-joist.

$$P_{cr} = \left(\left(\frac{24\pi^2 aEI_y}{(6+\pi^2)l^3}\right)^2 + \frac{EI_yGJ + \left(\frac{\pi hEI_y}{2l}\right)^2}{\frac{(6+\pi^2)l^4}{48\pi^4}}\right)^{\frac{1}{2}} - \frac{24\pi^2 aEI_y}{(6+\pi^2)l^3}$$

(6)

Where, a is the distance from the neutral axis to the point in which the load is applied. When the load is applied at the neutral axis, a equals zero. When a is zero, the accuracy of the remaining equation derived from the strain energy method was 1.0135 greater compared to the solution obtained by solving the system of differential equations of equilibrium. This accuracy was satisfactory for practical applications (Timoshenko 1936). The load was applied at the top flange of the wood I-joist so that a equaled $\frac{h}{2}$. Equation 6 accounts for the effects of the warping shear stresses. When the warping shear stresses from Equation 6 equal zero, the remaining equation equals the static critical lateral buckling load equation for a simply supported rectangular cross-section beams with the load applied at the top surface.

No research was found in the literature for the function β for the angle of twist for a fixed beam. The following function was derived considering the end support conditions from Equations 2.

$$\beta = \sum_{n=1}^{\infty} b_{(2n-1)} \cos\left(\frac{(2n-1)\pi z}{l}\right)^2$$

(7)

Equation 7 can be minimized in the same form as Equation 5. Considering that the load is applied at the mid-span ($s = \frac{l}{2}$) and using a single term for β from Equation 7, the following equation shows the static critical lateral buckling load was obtained for a fixed wood I-joist.

$$P_{cr} = \left(\left(\frac{64\pi^2 aEI_y}{(17+2\pi^2)l^3}\right)^2 + \frac{EI_yGJ + \left(\frac{\pi hEI_y}{l}\right)^2}{\frac{(17+2\pi^2)l^4}{128\pi^4}}\right)^{\frac{1}{2}} - \frac{64\pi^2 aEI_y}{(17+2\pi^2)l^3}$$

(8)

Comparing Equations 6 and 8, warping shear stresses were greater for the simply supported compared to the fixed wood I-joist. Solutions derived from the differential equations of equilibrium for the case of a fixed wood I-joist were not found in the literature and Equation 8 cannot be compared with exact solutions. Equation 8 accounts for the effects of the warping shear stresses. When the warping shear stress term from Equation 8 equal zero, the remaining equation becomes the static critical lateral buckling load equation for fixed rectangular cross-section beams with the load applied to the top surface.

No research was found in the literature for the function β for the angle of twist for a hanger fixed wood I-joist. Instead of deriving a new function for β, a previous equation was modified to account for the effects of the springs and Equation 5 was used for the function β. The work done by the springs W_s can be found using Equation 3 and the reaction at the end of the wood I-joist.

$$W_s = \frac{P^2(l-s)^2}{kl^2} \tag{9}$$

Adding Equation 9 to previous equations of lateral buckling work, the following equation was obtained.

$$\frac{P^2(l-s)^2}{kl^2} + \frac{Pa\beta^2}{4} + \frac{P^2(l-s)s}{EI_y l^2}\int_0^s \beta^2(s-z)^2 dz = GJ\int_0^s \left(\frac{d\beta}{dz}\right)^2 dz - \frac{EI_y h^2}{4}\int_0^s \left(\frac{d^3\beta}{dz^3}\frac{d\beta}{dz}\right)dz \tag{10}$$

Applying a load at mid-span ($s=\frac{l}{2}$) and using a single term for β from Equation 5, the following equation for the static critical lateral buckling load is obtained for a hanger fixed wood I-joist.

$$P_{cr} = \left(\left(\frac{24\pi^2 aEI_y}{(6+\pi^2)l^3 + \frac{48\pi^2 EI_y}{k}}\right)^2 + \frac{EI_y GJ + \left(\frac{\pi hEI_y}{2l}\right)^2}{\frac{(6+\pi^2)l^4}{48\pi^4} + \frac{lEI_y}{\pi^2 k}}\right)^{\frac{1}{2}} - \frac{24\pi^2 aEI_y}{(6+\pi^2)l^3 + \frac{48\pi^2 EI_y}{k}} \tag{11}$$

Where, k is the stiffness constant of the spring. As k approaches infinity, the spring becomes a rigid body and the simply supported case is attained (Equation 6). Equation 11 can be applied to different end support conditions by modifying the stiffness constant k of the hanger in the lateral direction.

Pseudo-dynamic loading refers to the loading applied by an individual walking on the wood I-joist under normal walking. Normal human walking is characterized by a smooth vertical rise and fall of the trunk, occurring once with each step or twice during a gait cycle (Gard and Childress 2001). In a normal human walking only one foot at a time leaves contact with the ground and there is a period of double-support (Pimentel et al. 2001).

The pseudo-dynamic lateral buckling models were developed by linearly combining the static lateral buckling models with the bending motion equations of the wood I-joists. The static lateral torsional buckling models used the total lateral displacement generated by the bending motion of the wood I-joists as initial conditions to find the critical lateral buckling position of the individual walking on the wood I-joists. The bending motion equations used the lateral component of the force F_L imposed by an individual walking on the wood I-joists to calculate the total lateral displacement of the wood I-joist under lateral buckling instability. Nakamura and Kawasaki (2006) found that the lateral component of the force F_L imposed by an individual walking under normal walking was of 10% of the vertical component while Huang et al. (2007) found that the same lateral component of the force was 4% of the vertical component. The

lateral component of the force F_L was used to account for the lateral pseudo-dynamic loading on the wood I-joist.

$$F_{dl}(t) = F_L G_W \left(1 + \sum_{n=1}^{m} \alpha_n \sin(2n\pi f_d t + \varphi_n) \right)$$

(12)

The bending motion of the wood I-joist was investigated for a distributed load. The lateral pseudo-dynamic loading in Equation 12 must be converted to a distributed load, by multiplying by the spatial Dirac Delta $\delta(z)$ function and the temporal Heaviside Theta $\Theta(t)$ function as shown in Equation 13.

$$f(z,t) = F_{dl}(t)\delta(z-s)\Theta(t)$$

(13)

When an individual walks on a wood I-joist, the lateral pseudo-dynamic loading from each footstep applied produces a unique solution for the wood I-joist bending motion since the lateral pseudo-dynamic loading is applied at a different point on the wood I-joist span. The mathematical description of the response of the wood I-joist to walking would require separate solutions from each footstep must be summed. This summation creates a complicated and cumbersome solution for the bending motion of the wood I-joist. The lateral pseudo-dynamic loading (Equation 13) was applied to the wood I-joist at mid-span. Then, the lateral pseudo-dynamic loading was adjusted by a function $g(t)$ in the time domain. This function simulated the average variation of the response of the wood I-joist to the individual walking. Adjusting functions were developed using the deflection curves when the wood I-joist was loaded at mid-span by a normalized concentrated load ($P = 1$). The adjusting functions were derived solving Equation 14 for each of the three end support conditions given by Equations 1, 2 and 4.

$$EI_y \frac{d^2 t}{dz^2} - M = 0$$

(14)

The adjusting functions comply with the physical characteristics of the response of the wood I-joist to the individual walking. The adjusting functions are zero at the ends, and gradually increase until a maximum value at the mid-span. The pseudo-dynamic lateral buckling model for a simply supported wood I-joist was derived to find the wood I-joist deflections produced by the individual walking. The lateral pseudo-dynamic loading $f(z,t)$ was applied from Equation 13. The spatial function $\chi_r(z)$ and the frequency of oscillation ω_r were calculated. The adjusting function $g(t)$ was derived by solving Equation 14 using the end support conditions from Equations 1. A normalized solution for a simply supported wood I-joist and for the first natural mode is shown.

$$\chi_r(z) = \sqrt{\frac{2}{ml}} \sin \frac{\pi z}{l}$$

(15)

The natural frequency of oscillation is given in the following equation.

$$\omega_r = \pi^2 \sqrt{\frac{EI}{ml^4}}$$

(16)

The adjusting function was derived for a simply supported wood I-joist from Equation 14.

$$g(t) = \frac{t(4t^2 - 3l^2)}{48EI_y}$$

(17)

Figure 20 shows the adjusting function from Equation 17 and the lateral pseudo-dynamic load history produced by an individual walking on a simply supported wood I-joist from Equation 12 modified by the adjusting function from Equation 17. The individual's weight G and the lateral bending stiffness EI_y of the wood I-joist were normalized to a maximum lateral pseudo-dynamic loading of one pound. Figure 20 can be compared with the pseudo-dynamic load history for one individual walking on a common surface.
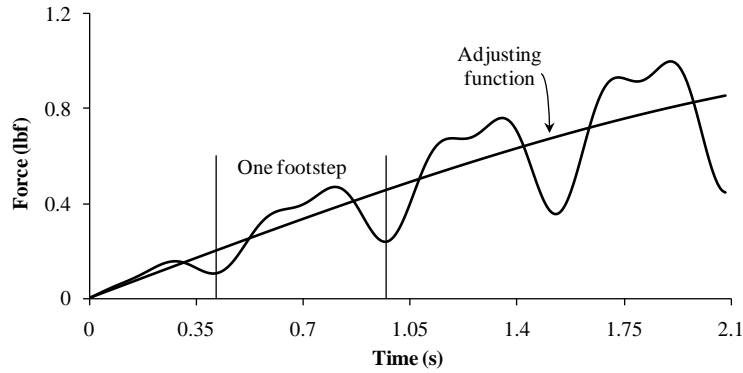

Figure 20. Lateral Pseudo-Dynamic Load History for an Individual Walking on a Simply Supported Wood I-joist Modified by an Adjusting Function

For a simply supported wood I-joist, the bending motion equation was developed. Equation 13 was substituted to account for the lateral pseudo-dynamic loading $f(z,t)$. The spatial function $\chi_r(z)$ was substituted from Equation 15. The frequency of oscillation ω_r was substituted from Equation 16. The adjusting function $g(t)$ was substituted from Equation 17. The bending motion equation for a simply supported wood I-joist is shown in Equation 18.

$$x(z,t) = -\frac{l^3\sqrt{2ml}\left(\cos\left(\frac{\pi^2 t\sqrt{\frac{EI_y}{m}}}{l^2}\right) - 1\right)g(t)F_{dl}(t)\chi_r(z)}{\pi^4 EI_y}$$

(18)

Equation 18 permits the calculation of the wood I-joist deflections when a test subject is walking on the wood I-joist for simply supported end conditions.

The pseudo-dynamic lateral buckling model for a fixed wood I-joist was derived to find the wood I-joist deflections produced by a test subject walking. The lateral pseudo-dynamic loading $f(z,t)$ was applied from Equation 13. The spatial function $\chi_r(z)$ and the frequency of

oscillation ω_r were calculated. The adjusting function $g(t)$ was derived by solving Equation 14 using the end support conditions from Equations 2. A normalized solution for a fixed wood I-joist and for the first natural mode is shown.

$$\chi_r(z) = \frac{\cosh\left(\frac{4.730z}{l}\right) - \cos\left(\frac{4.730z}{l}\right) - 0.982\left(\sinh\left(\frac{4.730z}{l}\right) - \sin\left(\frac{4.730z}{l}\right)\right)}{\sqrt{ml}} \tag{19}$$

The natural frequency of oscillation is given.

$$\omega_r = 22.37\sqrt{\frac{EI_y}{ml^4}} \tag{20}$$

The adjusting function was derived by solving Equation 14 for a fixed wood I-joist.

$$g(t) = \frac{t^2(4t - 3l)}{48EI_y} \tag{21}$$

Figure 21 shows the adjusting function from Equation 21 and the lateral pseudo-dynamic load history produced by an individual walking on a fixed wood I-joist from Equation 12 modified by the adjusting function from Equation 17. The individual's weight G and the lateral bending stiffness EI_y of the wood I-joist were normalized to a maximum lateral pseudo-dynamic loading of one pound. Comparing Figure 20 with Figure 21, Figure 21 showed smaller effects at the beginning of the graph of the lateral pseudo-dynamic load history. Both functions increased slower for fixed end support conditions compared to simply supported end conditions.
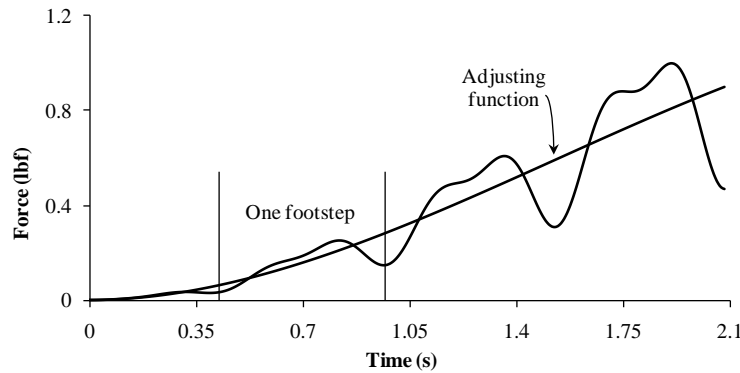
Figure 21. Lateral Pseudo-Dynamic Load History for an Individual Walking on a Fixed Wood I-joist Modified by an Adjusting Function

For a fixed wood I-joist, the bending motion equation was developed. Equation 13 was substituted to account for the lateral pseudo-dynamic loading $f(z,t)$. The spatial function $\chi_r(z)$ was substituted from Equation 19. The frequency of oscillation ω_r was substituted from Equation 20. The adjusting function $g(t)$ was substituted from Equation 21. The bending motion equation for a fixed wood I-joist is shown in Equation 22.

35

$$x(z,t) = -\frac{l^3\sqrt{ml}\left(0.003178\cos\left(\frac{22.37t\sqrt{\frac{EI_y}{m}}}{l^2}\right) - 0.003178\right)g(t)F_{dl}(t)\chi_r(z)}{EI_y} \tag{22}$$

Equation 22 shows the calculation of the wood I-joist deflections when a test subject is walking on a fixed wood I-joist. The wood I-joist deflection was inserted to calculate the pseudo-dynamic critical lateral buckling position of the individual walking on a fixed wood I-joist.

The pseudo-dynamic lateral buckling model for a hanger fixed wood I-joist was derived to find the wood I-joist deflections produced by the individual walking. The lateral pseudo-dynamic loading $f(z,t)$ was applied from Equation 13. The spatial function $\chi_r(z)$ and the frequency of oscillation ω_r were calculated. When applying the end support conditions given by Equation 4, the stiffness constant k of the spring remained in the spatial function $\chi_r(z)$ and the frequency of oscillation ω_r. The adjusting function $g(t)$ was derived by solving Equation 14 using the end support conditions from Equations 4. Also, the stiffness constant k of the spring remained in the adjusting function $g(t)$. A solution for a hanger fixed wood I-joist is shown.

$$\chi_r(z) = \frac{2Ak(R\sin z\psi + Q\sinh z\psi) + A\psi^3\left((R-Q)\cos z\psi + (R-Q)\cosh z\psi + (S-T)\sin z\psi + (S-T)\sinh z\psi\right)EI_y}{2kR + (S-T)\psi^3 EI_y} \tag{23}$$

Where, $Q = \sin l\psi$, $R = \sinh l\psi$, $S = \cos l\psi$ and $T = \cosh l\psi$. The constant A is to be determined when normalizing Equation 23. To calculate the term ψ, the transcendental equation for $l\psi$ in Equation 24 must be solved.

$$\psi^6(ST-1)EI_y^2 + 2k\psi^3(TQ-SR)EI_y - 2k^2QR = 0 \tag{24}$$

The frequencies of oscillation are given.

$$\omega_r = (l\psi)^2\sqrt{\frac{EI_y}{ml^4}} \tag{25}$$

The adjusting function was derived by solving Equation 14 for a hanger fixed wood I-joist.

$$g(t) = -\frac{24EI_y + 3kl^2t - 4kt^3}{48kEI_y} \tag{26}$$

For a hanger fixed wood I-joist, the bending motion equation was developed. Equation 13 was substituted to account for the lateral pseudo-dynamic loading $f(z,t)$. The spatial function $\chi_r(z)$ was substituted from Equation 23. The frequency of oscillation ω_r was substituted from Equation 25. The adjusting function $g(t)$ was substituted from Equation 26. The bending motion equation for a hanger fixed wood I-joist is shown in Equations 27a and 27b.

$$x(z,t) = -\frac{l^4 m \left(\cos\left(\frac{(l\psi)^2 t \sqrt{\frac{EI_y}{m}}}{l^2} \right) - 1 \right) g(t) F_{al}(t) \chi_r(z) \chi_r\left(\frac{l}{2}\right)}{(l\psi)^4 EI_y}$$

(27a)

$$\chi_r\left(\frac{l}{2}\right) = \frac{2A\left(\cos\left(\frac{l\psi}{2}\right) + \cosh\left(\frac{l\psi}{2}\right)\right)\left(-EI_y\psi^3 \cosh\left(\frac{l\psi}{2}\right)\sin\left(\frac{l\psi}{2}\right) + \left(EI_y\psi^3 \cos\left(\frac{l\psi}{2}\right) + 2k\sin\left(\frac{l\psi}{2}\right)\right)\sinh\left(\frac{l\psi}{2}\right)\right)}{EI_y\psi^3 (\cos l\psi - \cosh l\psi) + 2k\sinh l\psi}$$

(27b)

Equation 27a and 27b show the calculation of the wood I-joist deflections when the individual is walking on the wood I-joist for hanger fixed end support conditions. The wood I-joist deflection was used to find the pseudo-dynamic critical lateral buckling position of the individual walking on the wood I-joist when the wood I-joist was hanger fixed. When the stiffness constant k of the spring approaches infinity, Equations 23, 25 and 27 approximate Equations 15, 16 and 18, respectively. When k approaches infinity, the hanger fixed end support condition becomes the simply supported end condition.

Derivation of Bracing Contribution to Lateral Buckling

Three different lean-on bracing systems were used in this research: No-bracing, one mid-span brace, and two quarter-span braces. The models derived apply to all bracing systems. A single model was developed for each one of the three end support conditions. No research was found in the literature to describe mathematically the reactions that lean-on bracing systems have on the attached beams. Assumptions for the bracing models included: buckling of one main member required all main members to buckle with the same lateral displacement, all loads were within the elastic range of the materials, the bracing members were perfectly rigid and stiff, reactions at the bracing points were fully transmitted from one main member through the braces to the other main member, reactions transmitted through the braces were zero at the ends of the wood I-joist and had maximum effect at the loading point, the end support conditions were the same for all wood I-joists in the bracing system, all wood I-joists in the system had the same length and the bracing system was symmetric with respect to the mid-span of the wood I-joists. The total critical lateral buckling load P_{ct} for a wood I-joist with a bracing system was calculated by Equation 28.

$$P_{crt} = P_{cr} + \frac{x[w]}{x[z]}\left(\frac{\sum_{i=1}^{n} EI_{y_{bi}}}{EI_{y_l}}\right)$$

(28)

Where, $x[w]$ was the lateral deflection of the wood I-joist at the bracing point in which the load was being applied and $x[z]$ was the lateral deflection of the same wood I-joist but at the loading point, $EI_{y_{bi}}$ were the lateral bending stiffness of each wood I-joist braced to wood I-joist in which the load was applied, and EI_{y_l} was the lateral bending stiffness of the wood I-joist in which the load was applied. The $x[w]$ and $x[z]$ lateral deflections can be calculated solving the following differential equations

$$x[w] = EI_y \frac{d^2 x}{dw^2} - M = 0$$

(29a)

$$x[z] = EI_y \frac{d^2x}{dz^2} - M = 0$$

(29b)

Equations 29a and 29b must be solved along with the end support conditions for each case. To calculate the total critical lateral buckling load P_{crt} in a wood I-joist with a bracing system, the laterals bending stiffness of all wood I-joists in the system must be known.

Solving Equations 29 along with the end support conditions given by Equations 1, and inserting the solutions into Equation 28, the following equation was obtained to calculate the total critical lateral buckling load for a simply supported wood I-joist with a bracing system.

$$P_{crt} = P_{cr} + \frac{w(2ls - s^2 - w^2)}{2(l-s)s^2}\left(\frac{\sum_{i=1}^{n}EI_{y\,bi}}{EI_{y_l}}\right) \quad w < s$$

(30)

Where, P_{cr} is the critical lateral buckling load for the wood I-joist without the bracing system. P_{cr} for static loadings can be calculated for pseudo-dynamic loadings can be calculated using the procedure described previously. In Equation 30, w was the distance from the end of the wood I-joist to the bracing point and s was the distance from the end of the wood I-joist to the loading point (Figure 22).
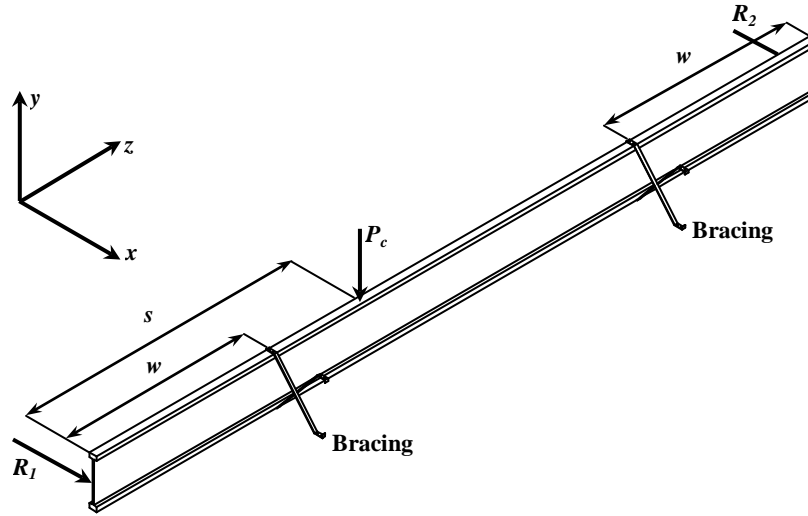
Figure 22. Wood I-joist with a bracing system

The term $\frac{w(2ls - s^2 - w^2)}{2(l-s)s^2}$ from Equation 30 equals 1.0 for the one mid-span brace and equals 0.6875 for the two quarter-span braces. Equation 30 demonstrated that a bracing system was more effective when applied at the mid-span compared to bracing applied away from the mid-span. For the one mid-span brace and assuming that the lateral bending stiffness of the three wood I-joists have the same value, the term $\frac{w(2ls - s^2 - w^2)}{2(l-s)s^2}$ proves that the total critical lateral buckling load for simply supported wood I-joists was three times larger compared with the critical lateral buckling load for the same wood I-joist without the bracing system, for the two quarter-span braces the difference was two times larger.

Solving Equations 29 according with the end support conditions given by Equations 2, and inserting the solutions into Equation 28, the following equation was obtained to calculate the total critical lateral buckling load for a fixed wood I-joist with a bracing system.

$$P_{crt} = P_{cr} + \frac{w^2(l(3s-w)-2sw)}{2(l-s)s^3}\left(\frac{\sum_{i=1}^{n}EI_{y_{bi}}}{EI_{y_l}}\right) \quad w < s \qquad (31)$$

The term $\dfrac{w^2(l(3s-w)-2sw)}{2(l-s)s^3}$ from Equation 31 equals 1.0 for the one mid-span brace and equals 0.5 for the two quarter-span braces. For the one mid-span brace and assuming that the lateral bending stiffness of the three wood I-joists have the same value, the term $\dfrac{w^2(l(3s-w)-2sw)}{2(l-s)s^3}$ proves that the total critical lateral buckling load for fixed wood I-joists was three times larger compared with the critical lateral buckling load for the same wood I-joist without the bracing system, for the two quarter-span braces the difference was 1.5 times larger. Lean-on bracing system is more restrictive for simply supported wood I-joists compared to fixed wood I-joists.

Solving Equations 29 along with the end support conditions given by Equations 4, and inserting the solutions into Equation 28, the following equation was obtained to calculate the total critical lateral buckling load for a hanger fixed wood I-joist when a bracing system is installed.

$$P_{crt} = P_{cr} + \frac{kl(l-s)w(2ls-s^2-w^2)+6EI_y(l^2+2sw-l(s+w))}{2\left(kl(l-s)^2s^2+3EI_y(l^2-2ls+2s^2)\right)}\left(\frac{\sum_{i=1}^{n}EI_{y_{bi}}}{EI_{y_l}}\right) \quad w < s \qquad (32)$$

The term $\dfrac{kl(l-s)w(2ls-s^2-w^2)+6EI_y(l^2+2sw-l(s+w))}{2\left(kl(l-s)^2s^2+3EI_y(l^2-2ls+2s^2)\right)}$ from Equation 32 equals 1.0 for the one mid-span brace and equals $\dfrac{11}{16}+\dfrac{15EI_{y_l}}{48EI_{y_l}+2kl^3}$ for the two quarter-span braces. From these results, it can be concluded that when the stiffness constant k of the spring approaches to infinite the term $\dfrac{kl(l-s)w(2ls-s^2-w^2)+6EI_y(l^2+2sw-l(s+w))}{2\left(kl(l-s)^2s^2+3EI_y(l^2-2ls+2s^2)\right)}$ approaches to 0.6875 which is the case for simply supported wood I-joists. Thus, the hanger fixed end support condition can be bounded by the simply supported end condition.

Conclusion of Theoretical Models

Static lateral buckling models were developed for each of the three end support conditions: simply supported, fixed and hanger fixed. Hanger fixed end support condition was derived to include many wood I-joist hangers found in the residential construction industry. The pseudo-dynamic lateral buckling models were developed combining the static lateral buckling models with the bending motion equations. The bending motion equations used the lateral component of the force imposed by an individual walking on the wood I-joists. The static and pseudo-dynamic lateral buckling models were applied to the three different bracing systems.

The bracing models describe the amount of bracing restrain on the lateral buckling instability. The bracing models were developed for each of the three end support conditions. (NOTE: Because of unforeseen student scheduling conflicts, the theoretical models were not validated as the finite element model was. This will be a priority in future research since the theoretical models seem promising to provide a more closed form solution to the challenge of lateral buckling and bracing).

Specific Aim #3

The ultimate goal and greatest impact of this research is in the development of safety strategies to help prevent falls from lateral buckling. Based upon the results of Specific Aims #1 and #2, safety strategies to prevent workers from accessing beams where lateral buckling can occur were formulated. The safety strategy seen as most effective during the Specific Aims #1 and #2 work was to provide additional bracing. Temporary bracing elements applied at the top flange can be manipulated by workers to reduce the unbraced length and reduce the hazards associated with lateral buckling. An intellectual property concept for a temporary joist stabilizer was developed. Previous research on the use of bracing of beams exposed to lateral buckling has focused on the loads that the joist is able to carry. No research has examined the movement, including the lateral displacement, twist and lateral acceleration, for different bracing placement and bracing stiffness.

Intellectual Property for Temporary Joist Stabilizer

An intellectual property (IP) entitled "Temporary Stabilizer for Wood Joist Installation" disclosure #08-035 was filed with the Virginia Tech Intellectual Properties (VTIP) department. Figure 23 shows the temporary joist stabilizer concept. A strongback – aluminum or steel channel – extends across several joists. The flanges shown in Figure 23 are duplicated for each joist. As the stabilizer is pressed onto the joist, the spring loaded left side allows the joist to enter the holder and provides a positive pressure to keep the joist in the fixture.
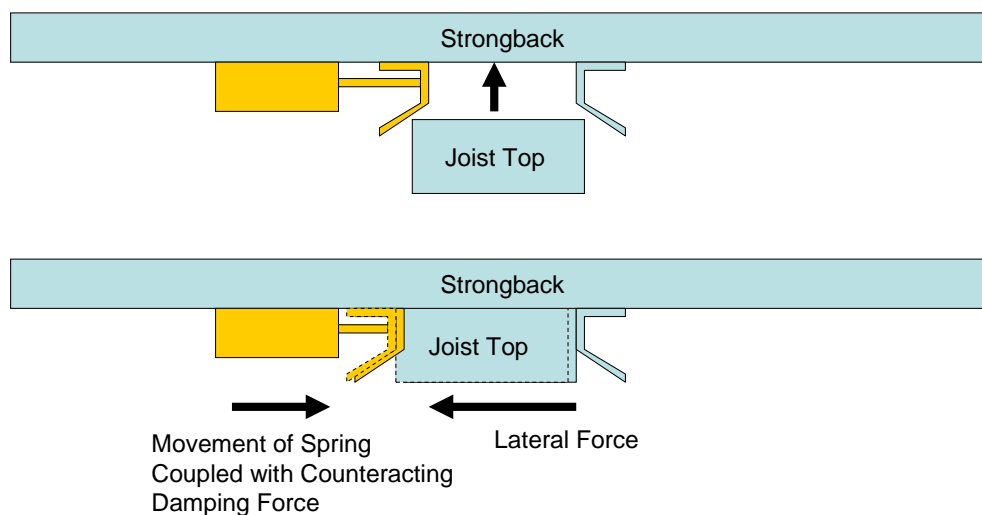
Figure 23. Temporary Joist Stabilizer Concept Applied for Intellectual Property Disclosure

Effects of Bracing Stiffness and Configuration

For this experiment, human test subjects walked across a wood composite I-joist. Different bracing stiffness and configurations were used, with a control of no bracing for comparisons. Accelerometers and string potentiometers were installed on the I-joist at different points of interest to record the I-joist's mechanical behavior. Results from testing measured the I-joist's lateral acceleration, lateral displacement and twist to determine the role of bracing in mitigating lateral movement.

The different test setups consisted of changing the stiffness as well as the configuration (spacing). To simulate bracing, the bracing devices described earlier were attached to the top flange every 60 in. and then every 80 in. All five stiffnesses (0 lb/in., 1.2 lb/in., 8.5 lb/in., 14.0 lb/in. and ∞ lb/in.) were tested with the two different configurations. Figure 24 displays the layout of sensors and bracing on the I-joist. "Bracing Points" denotes where bracing was attached and "Points of Interest" denotes where accelerometers and string potentiometers were located. In addition, Table 5 shows the different combinations tested and the number of tests performed for each combination. Test setups A and F are the control samples.
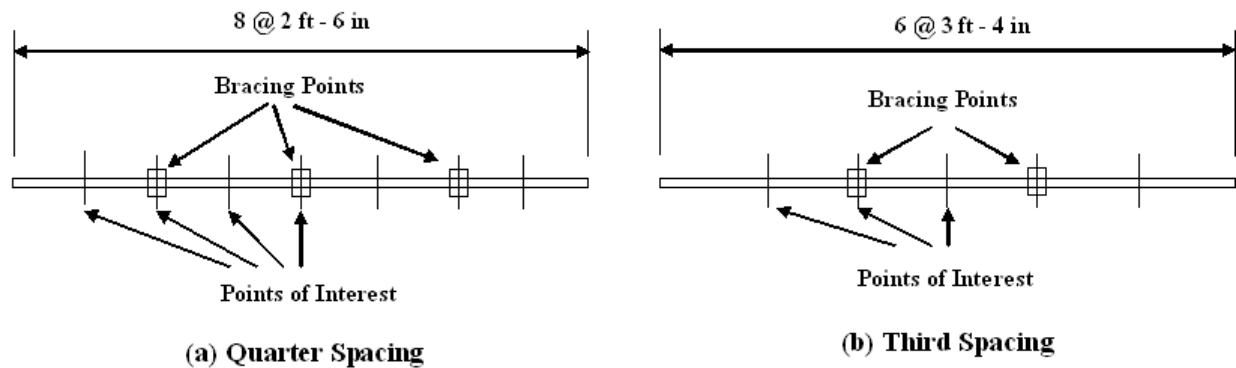
Figure 24: Placement of Sensors on I-joist

Table 5: Testing Layout

Test	Spring Stiffness (lb/in.)	Bracing Device Configuration	Number of Test Subjects
One-Quarter Span Length Spacing (60 in.)			
Test Setup A	0.0	---	10
Test Setup B	1.2	60 in	10
Test Setup C	8.5	60 in	10
Test Setup D	14.0	60 in	10
Test Setup E	∞	60 in	10
One-Third Span Length Spacing (80 in.)			
Test Setup F	0.0	---	10
Test Setup G	1.2	80 in	10
Test Setup H	8.5	80 in	10
Test Setup I	14.0	80 in	10
Test Setup J	∞	80 in	10

The test subjects were equipped with a tool belt with up to 9.6 lbs of common tools to simulate additional weight and eccentricities while walking across the I-joists. The test subjects consisted of 14 students and 6 construction workers. Students were male Virginia Tech graduate students between the ages of 22 and 25, with one student being 30. Construction workers were recruited from two different contractors. All were male with ages ranging from 23 to 36. The population of test subjects included those familiar with walking on I-joists as well as those unfamiliar with walking on I-joists. Each test subject was given a unique identification number for each test (1-10 for the 60 in. brace configuration and 21-30 for the 80 in. brace configuration). All subjects were secured by a safety harness attached to the safety platform while walking

across all testing. The test subjects were asked not use the hand rails as support unless they lost their balance to prevent the dispersal of body weight to the hand rail, thereby reducing the load applied to the I-joist. The tests subjects were asked to walk to an electronic metronome at a beat of 45 steps per minute so that a constant walking speed would be used throughout testing. All testing conformed to standards of the Virginia Tech Institutional Review Board (IRB) for using human subjects. Figure 25 shows a picture of a test subject walking across the I-joist while attached to the safety platform.

Figure 15: Test Subject Walking Across the I-Joist

Once the test subjects walked across each test setup, they were asked to fill out a survey that inquired as to the difficulty of walking on the I-joist. Questions included whether walking was made more difficult closer to the bracing points or in the middle of the bracing points, as well as open-ended questions about their opinions. After each participant had walked all five test setups for each spacing, they were asked on a scale of 1-5 how much the bracing improved the ease of walking on the I-joist. They were also asked at what bracing they began to feel comfortable, if the walking speed designated was too fast and asked to provide any additional comments. In addition, the subjects were asked to record their weight, height, age, ethnicity and occupation on the survey as well.

The safety platform used in Specific Aim #1 was used for all bracing testing. Figure 26 shows the end supports constructed. Three GP16 I-joists were placed longitudinally parallel inside of the safety platform and supported by built-up end supports. A span of 20 ft was used and attached with face mount joist hangers to simulate a simply supported connection. The hangers were supported by and connected to an LVL end support which simulated a rim board as a rigid member. Since bracing stiffness and spacing were studied, only the middle I-joist mechanical behavior was recorded and analyzed.

(a) I-Joist Layout   (b) End Supports
Figure 26: I-Joist Layout and End Supports

Five different bracing stiffness values were used including a control of no bracing, a solid bar representing an infinite stiffness and three intermediate stiffness values created by compression springs. Three different compression springs with varying stiffness were used including 1.2 lb/in., 8.5 lb/in. and 14.0 lb/in. The springs were covered by rigid tubing during testing to prevent buckling. The bracing device connected the compression springs to the I-joist and was fabricated from steel channel. A ½ inch diameter bolt was used to tighten the bracing against the top flange. The springs were attached to the bolts through pinning or welding, depending on the spring size. Spring stiffness was verified by an MTS Universal Testing Machine. The infinitely stiff spring consisted of a ½ in. diameter threaded steel rod with a stiffness of approximately 400,000 lb/in. (considered to be infinite)

Bracing devices were spaced along the I-joist at two different configurations (spacings); one-quarter and one-third of the span length or 60 in. and 80 in. respectively. These brace configurations were chosen as commonly used spacings.

Accelerometers and string potentiometers measured the mechanical behavior of the I-joist. Three accelerometers from PCB Piezotronics, Inc. and were analyzed in RT Pro (5.5, LDS/SPX, Fremont, CA). The string potentiometers were string fed, spring loaded, and had a range of up to 8 in. with a sensitivity less than 1% and allowed for readings of up to 4 in. in each direction.

The accelerometers and string potentiometers were installed at each point of interest along the I-joist. Potentiometers were placed at the top and bottom flange, while the accelerometer was placed at the top flange also. Lateral displacement was measured from the top potentiometer. Twist was measured from the trigonometric relationship of the top and bottom flange potentiometers. Continuous readings were taken as each subject walked across the I-joist and stopped once each test subject reached the opposite end of the I-joist. Sensors were only installed on half the I-joist since the behavior was assumed to be symmetrical about mid-span. Once the data from the accelerometers and string potentiometers were measured, the largest lateral acceleration, lateral displacement and twist at each point of interest for each brace stiffness and configuration were retrieved. This was done for each test subject and yielded a total of 350 data points for each mechanical behavior - 200 for the 60 in. bracing configuration and 150 for the 80 in. bracing configuration.

Once all the data were extracted, separate Analyses of Covariance (ANCOVA) for each mechanical behavior were performed using JMP® (7.0.1, SAS, Cary, NC) to assess the effects of brace stiffness (five levels), brace location (seven levels, i.e. four locations for the 60 in. brace configuration, three locations for 80 in. brace configuration) and participant reaction on the I-

joist movement (lateral acceleration, lateral displacement and twist). A mixed-factor fixed-effects model was used, with brace stiffness and configuration as within-subject factors and occupation as a between-subjects factor. Body weight was also included as a continuous covariate. Table 6 shows the model that was input into JMP®. The "[ ]" denotes that factor is nested while "x" denotes that the factors are crossed.

Table 6: Statistical Model Summary

Independent Variables	Dependent Variables
Occupation	Lateral Accelerations
Subject $_{Random\ Effect}$ [Occupation]	Lateral Displacements
Weight	Twist
Location	
Stiffness	
Location x Stiffness	

To achieve normality, each of the dependent measures was log transformed prior to analysis; however, summary of the statistics were provided in the untransformed values. Also, a visual inspection check was performed for outlying measures. One outlying measure was found for subject 30 at the mid-span location for the 80 in. brace configuration. Additional analyses confirmed that including this outlier did not change the major results reported. Post-hoc pairwise comparisons were done using the Tukey's HSD and several contrasts were used to assess the effects of brace configuration. Results from all statistical analyses were considered significant when $p < 0.05$.

Results and Discussion

Specific Aim #1

Figure 27 shows two pictures which were taken from the site visits. A total of four visits at two different construction sites were conducted. Due to the infrequency of I-joist construction used in the Blacksburg area, some observations included the construction of solid wood floor and roof systems. Figure 27a shows workers standing on the top plate of the wall and the edge of the trusses placing the fascia board on the end of the trusses. Figure 27b shows some of the loads that workers would have to carry as they moved across the floor and roof systems. The worker on the left is carrying a nailgun and the worker on the right has a 4x8 sheathing panel. Both of these workers are carrying heavy, off balanced loads. The tools and materials workers need to work on unbraced systems such as floors and roofs can further challenge their balance. Off-center loading can lead to more frequent losses of balance. Compensation for these loss of balance incidents can lead to worker fatigue and increased concentration to prevent falls. The observations of jobsites confirmed the need to develop strategies for lateral buckling. Also, the need to introduce off-balance loading of the workers in the laboratory environment was an important component to developing realistic balance conditions.

| (a)   (b) |

Figure 27: Field Observations of Workers Walking on Individual Wood Elements

Static Loading Results

      This section compared the lateral displacement of the top and bottom flanges, as well as the rotation, at both the midpoint and quarter point to examine any significant differences between test replications and different joists of the same size. For dependent variable comparison, lateral displacements and rotations were analyzed separately to test for any significant differences. Five joists of each of the three sizes were tested six times, for a total ninety bending tests.

      Data was collected up to 500 lbs for the GP14 joists, 350 lbs for the GP12 joists, and 250 lbs for the TJI12 joists. This load range was based on the amount of slip that occurred during each test and the lateral/rotational stiffness of the joist size. As the load increased, the frictional force between the bearings and the metal plate became greater. This created larger 'slips' in lateral deflections at higher loads; the slips in deflection are relative to the amount of load applied to the beam. A typical load-deflection curve is shown in Figure 28. Note that larger 'slips' in deflection occured at higher loads. In an idealized test, there would be no deflection slips. When the deflection slips occur in the actual test, the built up frictional force is released and the joist slips past the position in an ideal test. The force then has to build up above the idealized force-deflection curve before the next slip occurs. The regression line indicates a linear force-deflection curve.
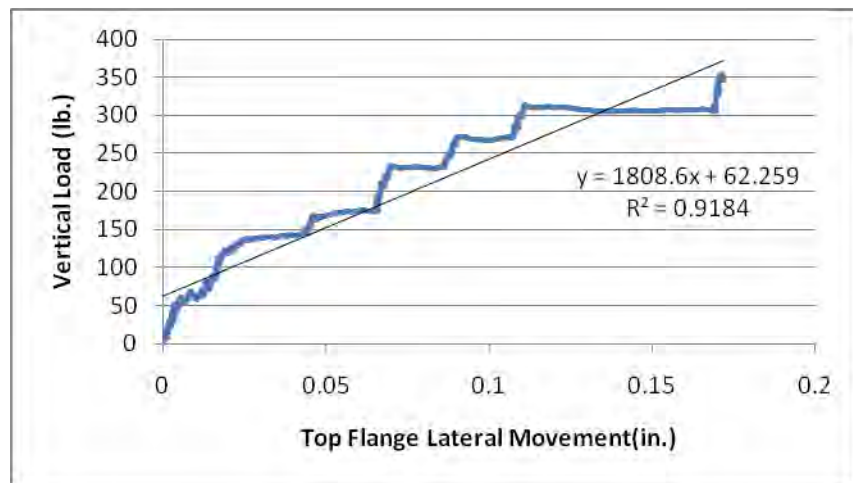

Figure 28. Typical Load-Deflection Curve

Table 7 shows the mean stiffness values and the coefficients of variation (COV) for each joist. The GP14 joists were the stiffest joist type followed by the GP12 and TJI12 joists. Some joists such as the GP14-3 and TJI12-2 have a noticeably greater average value; however, the COV for these joists was also greater. Stiffer joists exhibited a wider variation of stiffness values. There is a considerable amount of variation in the COV values within each joist type. More joists may provide generalized results within an entire joist type. The rotational stiffness of the joists exhibited lower COV values compared to the top and bottom flange lateral displacement. The top flange of the beam had lower COV values than the bottom flange, indicating a more consistent performance. These deflection trends were apparent in both the midpoint and the quarter point measurements. All quarter point measurements exhibited lower variation than the midpoint measurements.

Table 7. Lateral/Rotational Stiffness of Joists

	Lateral / Rotational Joist Stiffness (lb/in)												
	Midpoint						Quarter Point						
Joist	Top Flange		Bottom Flange		Rotation (lb/deg.)		Top Flange		Bottom Flange		Rotation (lb/deg.)	
	Mean	COV	Mean	COV	Mean	COV	Mean	COV	Mean	COV	Mean	COV
GP14-1	1232	8.0%	1712	11.1%	485	3.3%	1605	7.6%	2730	11.5%	2454	1.2%
GP14-2	2872	8.3%	3581	10.2%	1541	5.9%	3854	7.4%	5658	10.2%	2011	1.6%
GP14-3	2315	12.6%	5281	19.4%	472	3.1%	2872	10.6%	8833	18.0%	2380	2.1%
GP14-4	2000	3.7%	2944	4.7%	915	4.4%	2890	3.4%	4850	4.7%	2233	2.3%
GP14-5	1297	4.7%	1735	4.1%	659	4.8%	1818	5.6%	2859	5.0%	2200	1.4%
GP12-1	943	5.0%	800	5.4%	545	3.8%	1327	4.5%	1627	4.9%	1424	1.5%
GP12-2	1129	12.6%	918	13.1%	791	19.8%	1655	11.9%	1959	13.4%	1334	2.2%
GP12-3	1434	5.5%	1488	7.5%	457	3.3%	2182	5.5%	3553	8.6%	1518	1.8%
GP12-4	936	9.1%	816	11.6%	506	4.9%	1394	8.8%	1819	10.4%	1480	1.6%
GP12-5	1355	2.6%	1207	2.5%	541	1.8%	1915	2.4%	2620	3.1%	1524	1.3%
TJI12-1	541	18.2%	510	8.1%	217	16.6%	723	17.3%	1078	18.0%	1082	3.8%
TJI12-2	1017	33.5%	996	41.5%	279	7.3%	1396	28.8%	2573	55.5%	1136	3.2%
TJI12-3	804	10.0%	685	12.5%	353	5.5%	1111	9.7%	1578	14.0%	1088	0.4%
TJI12-4	412	10.7%	368	11.9%	195	6.6%	585	11.0%	833	12.4%	1135	0.9%

The stiffness data was then examined using a random-effects analysis of variance (ANOVA), to assess whether there were significant differences between joists of the same type and replications within a given joist. Table 8 shows no significant differences between replicate tests on the same joist. However, significant differences did exist between all joists of the same size. This verifies the previously discussed trend that a larger sample is needed to characterize a given joist type.

Table 8. Comparison of the Joist and Replications Used for Static Loading[1]

Joist Type	Factor	Midpoint			Quarter		
		Top Flange	Bottom Flange	Rotation	Top Flange	Bottom Flange	Rotation
GP14	Joist	0.0001	0.0001	0.0001	0.0001	0.0001	0.0001
	Replication	0.4953	0.4057	0.8916	0.6200	0.4412	0.5265
GP12	Joist	0.0001	0.0001	0.0001	0.0001	0.0001	0.0001
	Replication	0.2402	0.3822	0.3552	0.3070	0.4009	0.1957
TJI12	Joist	0.0001	0.0009	0.0001	0.0001	0.0045	0.0037
	Replication	0.3601	0.4739	0.2146	0.3767	0.4507	0.3394

[1] Highlighted cells indicate $p < 0.05$

Since the difference within the replications was not significant, the data was analyzed using a single factor, random-effects ANOVA to identify the components of variance related to differences between joists of a given type and within a given joist. The percent variance attributed to the joist and residual effects are shown in Table 9. The less rigid joists, such as the TJI12, had a higher proportion of the total variance related to within-joist variability. These higher residual values indicate larger amounts of variation within joist types. Since less rigid joists were more susceptible to outside effects, slight misalignment of the joist underneath the load cell or friction forces generated in the bearing support beneath the load cell was critical to obtaining accurate measurements of the lateral displacements and rotations.

Table 9. Percentage of Variance Attributed to Joists and Residual Error Sources

Joist Type	Variance Component	Midpoint			Quarter		
		Top Flange	Bottom Flange	Rotation	Top Flange	Bottom Flange	Rotation
GP14	Joist	93.698	89.697	98.868	95.214	90.993	94.810
	Residual	6.302	10.303	1.132	4.786	9.007	5.190
GP12	Joist	87.506	91.810	75.466	89.496	93.514	91.146
	Residual	12.494	8.190	24.534	10.504	6.486	8.854
TJI12	Joist	66.789	59.117	89.719	72.653	48.549	48.146
	Residual	33.211	40.883	10.281	27.347	51.451	51.854

The results of the static test indicated that the joists tested were repeatable in their performance. However, due to the variability within a joist type, more joists are needed to fully characterize and entire joist type. Due to time limitations of this project, only three joists from each type could be tested dynamically. This will not undermine the validity of the ANSYS model, but more testing is required to validate the model for an entire joist type.

Dynamic Loading Results

Figure 29 shows the relationship between the weight of the test subject and maximum induced load on the top flange. A linear regression was fit for each joist type. The GP12 and GP14 I-joists have similar values and regressions. There is a significantly greater amount of variance within the TJI12 joists than the other two joist types. These dynamic loading results show the difference between the TJI12 and the other I-joists which was similar to the differences noted in the static loading.
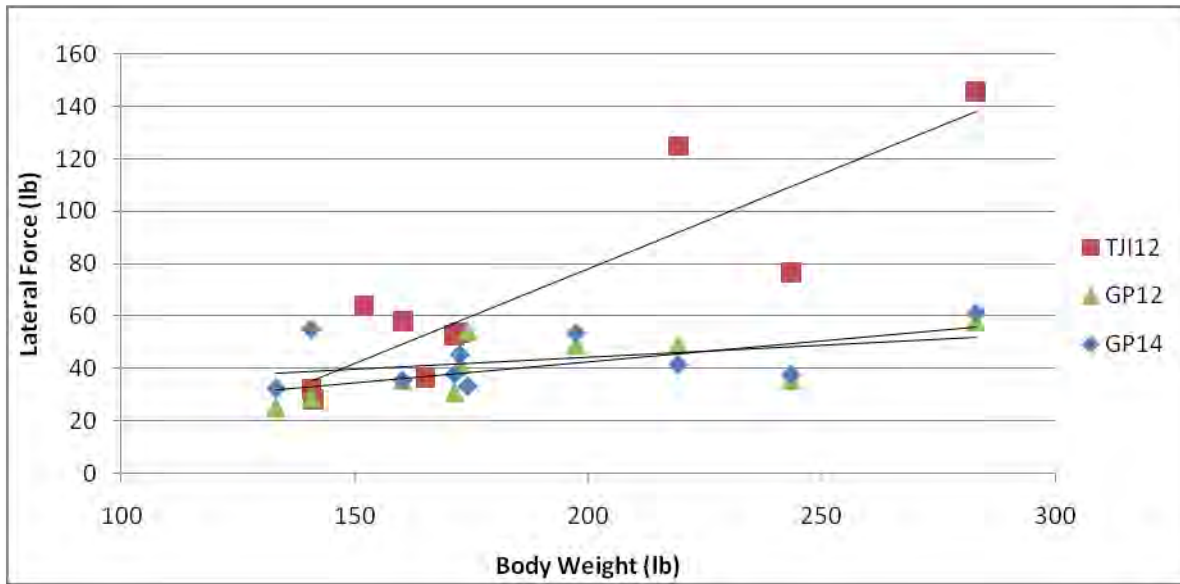
Figure 29. Body Weight versus Maximum Applied Lateral Load on Top Flange

Table 10 shows the slopes of these regression lines from Figure 29 and corresponding coefficients of determination, r^2, as well as the lateral and polar moment of inertia. The lateral and polar moments of inertia were calculated by assuming the material was isotropic, which provides a rough estimate of the LVL and OSB orthotropic materials. The lateral and polar moments of inertia are useful to compare the rotational stiffness of each joist type. The GP14 joists were the stiffest joists with respect to lateral and rotational stability, while the TJI12 joists were the least stiff. Although the low r^2 values for the two GP joist types indicate that a linear regression may not be a suitable fit to the data points, there appeared to be a trend among the weight of the test subject, the maximum applied lateral force, and the joist type. In general, as the weight of the test subject increased, the maximum applied lateral force also increased. The dramatically different slope value for the TJI12 joist (0.721 vs. 0.93 or 0.161) showed the TJI 12 joists had a much greater tendency to produce lateral load. Since the TJI12 joists were also longer than the GP12 and GP14 joists, clear conclusions about changes in the length or manufacturer of joist are not possible from this work. From the two 20 foot joists (GP12 and GP14), the lateral load averaged 12.7% of the static weight of the test subjects. Previous studies by Nakamura and Kawasaki (2006) and Huang et al. (2007) compared the lateral force of normal walking to the vertical force component rather than the static weight value. These studies found that lateral forces ranged from 4% (Huang et al. 2007) to 10% (Nakamura and Kawasaki 2006) which seem to be lower than current results if the static weight is considered the vertical force component, which depends heavily upon individual test dynamic factors.

Table 10. Trends in Body Weight and Applied Lateral Force

Joist Type	Slope	R-Squared	Lateral Moment of Inertia ($in.^4$)	Polar Moment of Inertia ($in.^4$)
GP14	0.093	0.20	3.19	243.8
GP12	0.161	0.45	3.18	208.9
TJI12	0.721	0.78	2.77	201.6

Figure 30 shows a typical response of the top and bottom flange load cells measured as a test subject walked across the joist (note that the horizontal axis is the time, not the distance). The top and bottom flange load cells did not measure similar load values. Since the load was applied at the top flange, this may explain the higher top flange load cell. The load cells placed on the end supports attempted to capture the induced effects caused by the weight of the test subjects and divided the load into three components. In order to fully capture the induced loads, readings would have to be taken at the test subject's feet utilizing triaxial load cells. This method would prove technically difficult and time consuming. The load values were similar at the beginning and conclusion of the test, indicating that the load may have dispersed through the joist as the test subject traveled through the beam to the load cells. Second order effects were also present due to the loading of the I-joist away from the shear center, as well as a constantly changing center of mass of the test subject from walking. The graph also illustrated the vibration effects that occurred in the latter half of the beam represented by the closely spaced half-waves.
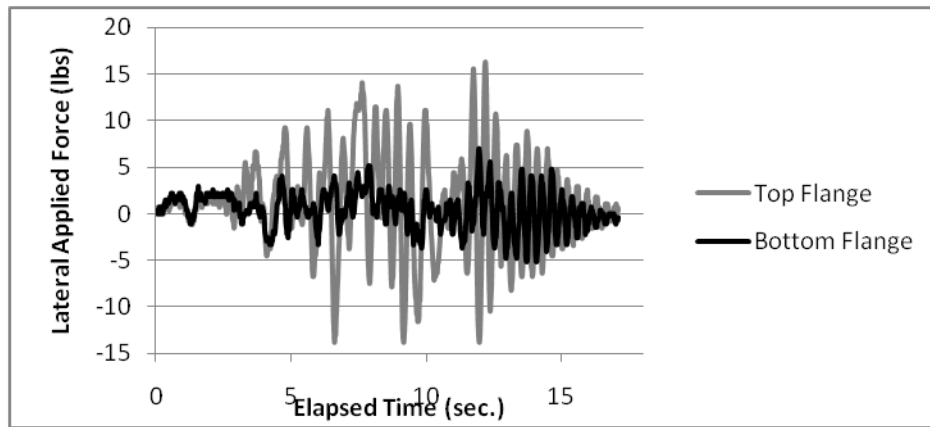

Figure 30. Variation of Top and Bottom Load Cell Readings

The relationship between body weight and maximum deflection was also of interest. Figure 31 depicts each test subject's average maximum lateral deflection from the mid-span top flange data over the six trials for each joist type and their corresponding weight. The slopes from the GP12 and GP14 were 0.008 and 0.007 respectively, while the slope for the TJI12 joists was considerable higher at 0.034. This change is slope may be due to the longer length of the TJI12 or due to the different manufacturer. These results are confounded between the different lengths and manufacturers and require further investigation to understand the different variables. An ANOVA was also conducted with these results and no significant difference of the test subject's weight or joist type was found for the recorded deflections.
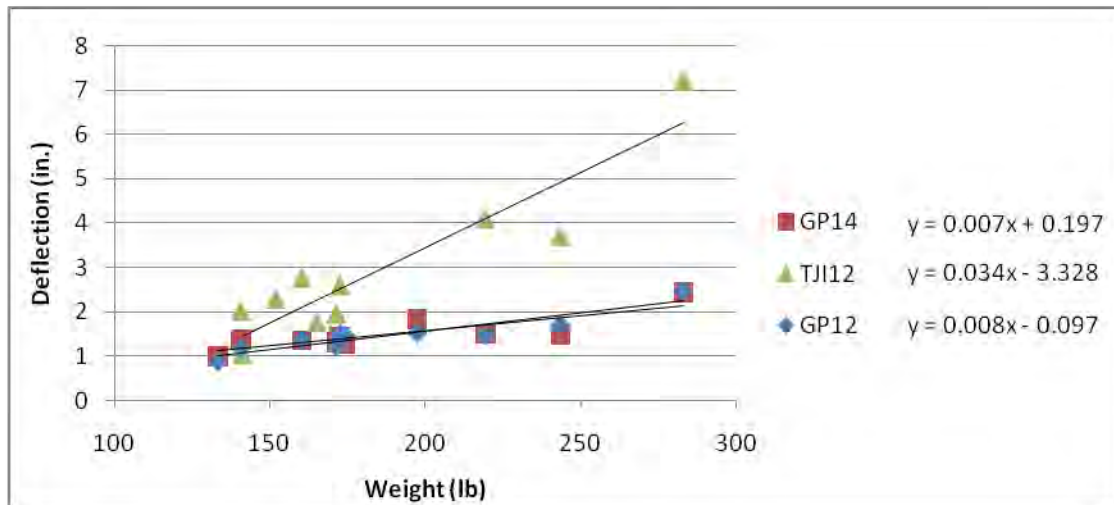
Figure 31. Average Maximum Deflection of Top Flange

The results of the dynamic test indicated that there is a strong relationship between the overall stiffness of the I-joist and the maximum load induced by the test subject. The results also indicated a strong relationship between the test subject's weight and the maximum applied load and maximum deflection of the joist. For the two GP joists tested at common lengths, the average lateral load was 12.7% of the test subject's static weight. More specific conclusions are difficult to find due to the confounding effects of joist length and joist manufacturer.

Specific Aim #2

Finite Element Model Results

The full pseudo-dynamic analysis was compared to the acquired test data by the amount of error between the two maximum value curves (MVC). The MVC is generated from taking the magnitude of the largest values from a deflection curve; the full development is illustrated by Figure 32. The raw data is first normalized to an initial displacement of zero, Figure 32(a). The absolute value of this curve generates the absolute value curve seen in Figure 32(b). To create the MVC, Figure 32(c), only increasing data points were taken until the peak value; this process was applied from both ends of the graph.
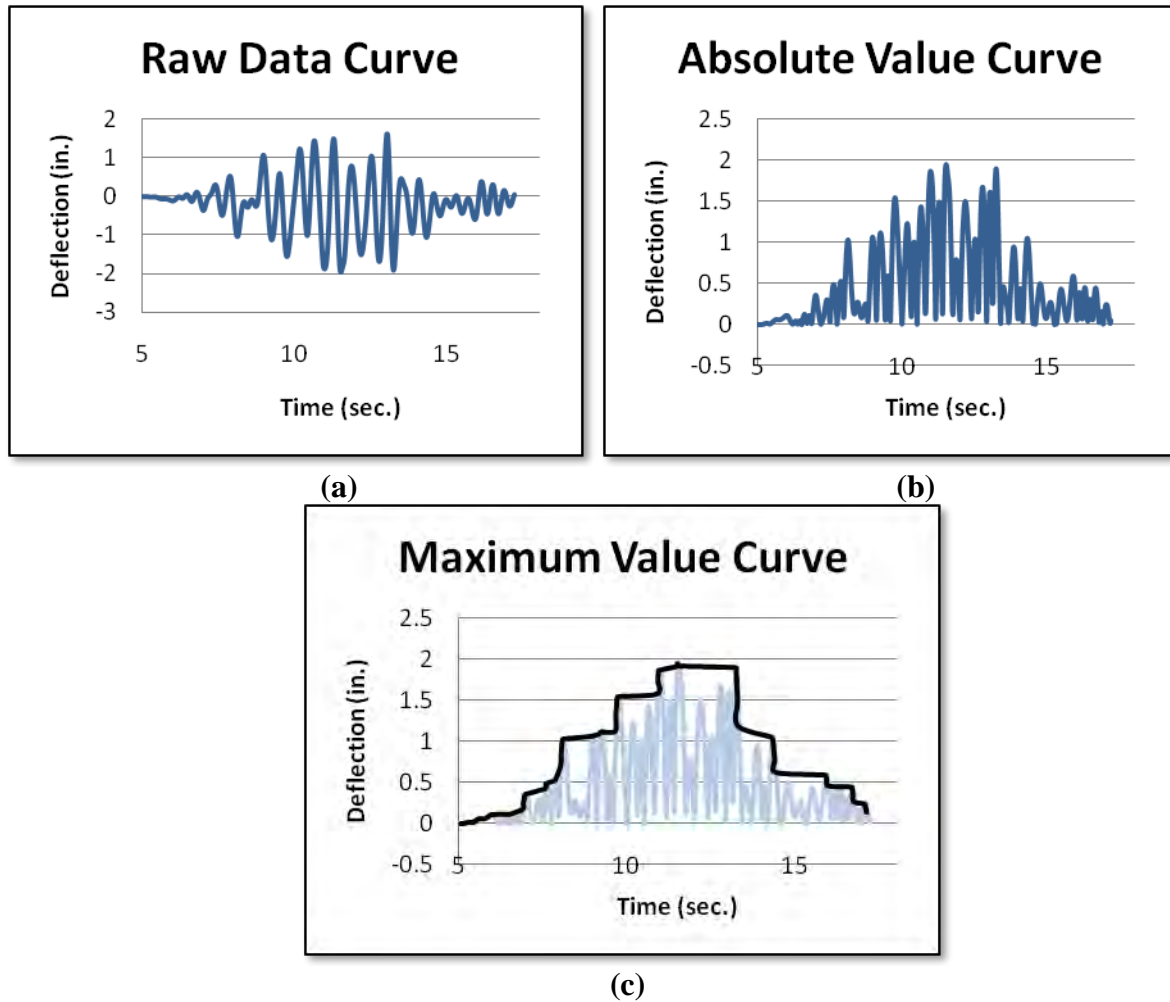
Figure 32. Development of the Maximum Value Curve

The data from the full pseudo-dynamic test was analyzed using two separate procedures. The first method compared the error between the two MVCs and compared the shapes of the curves. The second analysis focused on the peak values and the time at which they occurred. Figure 33(a) shows a typical MVC from the acquired data and the corresponding values generated from ANSYS. The time scale for the graphs was converted to a percent of beam length for statistical comparison within joist types. The absolute value of the difference between the two curves was computed on a point-by-point basis and a running average was calculated. Figure 33(b) depicts the average cumulative error between the two curves.
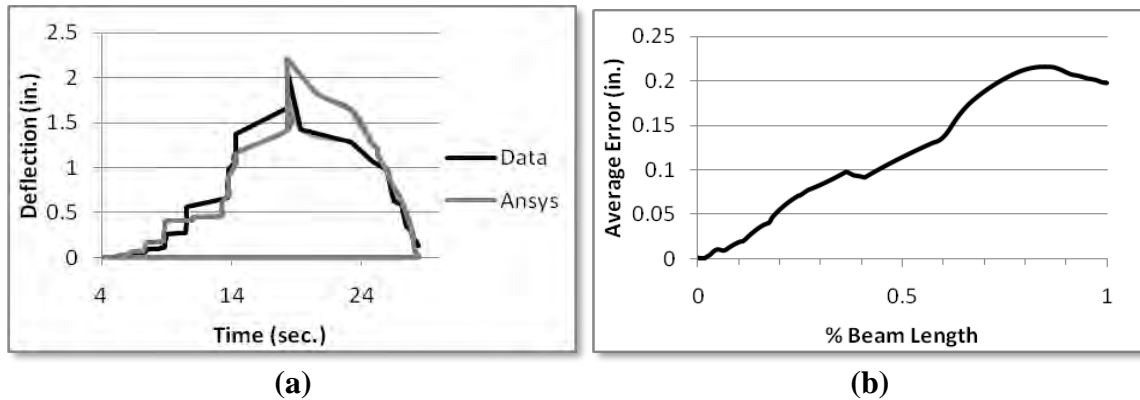
(a)   **(b)**

Figure 33. (a) MVC for Acquired Data and ANSYS Model (b) Average Error in Model

       A pair of curves was generated for each recorded deflection and calculated rotation, each test subject, and each experimental replication. The allowable amount of error was arbitrarily set to 10 percent of the maximum recorded deflection for each pair of curves. Once the amount of error exceeded 10 percent, the percent of beam length reached was recorded. During some comparisons, the maximum amount of error was exceed and then decreased below the threshold of 10 percent. This was not factored into any of the analysis; once the limit was reached, the comparison was concluded.

       In almost all instances, the model diverged at some point from the experimental data by more than 10 percent. During the acquisition of data, the vibration of the joist created additional deformations and lateral loads. This influence was concentrated on the latter half of the beam. Therefore, a percent length value of 50 percent was considered a good model. On several recorded data sets, deflections recorded at the test conclusion indicated that the beam was still in motion when the test subject stepped off. From visual observations after the test subject removed their weight, the joist entered a state of free vibration.

       Table 11 shows the percent of beam length when the difference of the model and experimental results exceeded the 10 percent limit. Although the top and bottom flange deflections generated by ANSYS for a particular analysis fit the experimental test data well, the corresponding rotation of the beam was not be a good fit. The rotations were calculated on a point-by-point basis from the ANSYS data and the maximum rotation may not have occurred at the time of maximum lateral displacement. The finite element model was able to predict the average deflections and rotations of the GP12 and GP14 joist with the stated 10% average error until 54.5% and 51.2% of the beam length, respectively. However, the model was only able to predict the average TJI12 movements until 31.2% of the beam length. The model predicted the lateral displacement of the top flange of the beam, regardless of location, the best, followed by the rotation and bottom flange displacement. An ANOVA was conducted to detect the differences due to the location of measurement on the percent of beam that passed. The results of the test showed no significance difference between the midspan and quarter point values.

Table 11. Percent of Beam at which Model No Longer Corresponds to Test Data

Joist Type	Midpoint			Quarter Point			
	Top Flange	Bottom Flange	Rotation	Top Flange	Bottom Flange	Rotation	Average
GP14	59.7%	47.9%	61.1%	46.8%	46.9%	44.5%	51.2%
GP12	60.0%	49.6%	68.0%	38.8%	60.2%	50.2%	54.5%
TJI12	39.5%	23.8%	40.2%	18.7%	35.0%	29.9%	31.2%
Average	53.1%	40.4%	56.4%	34.8%	47.4%	41.5%	

In addition to determining the time at which the model no longer fit the acquired data, the peak values of each curve and the corresponding time in the peak values were compared. This statistical analysis determined how well the model predicted the peak value with respect to time. The respective points compared on the curves for the ANSYS model and experimental data are shown in Figure 34. For the statistical analysis, the variables of Time and Value (deflection or rotation as appropriate) and were calculated for each lateral displacement and rotation recorded.
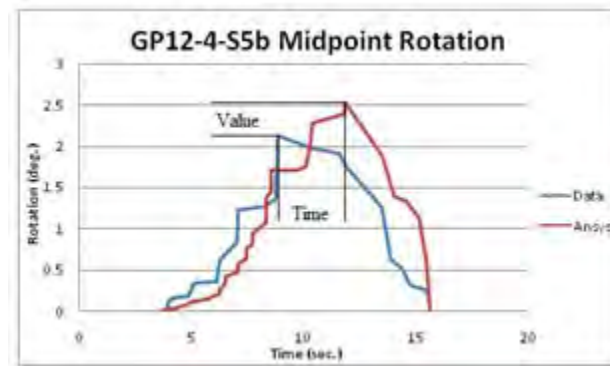

Figure 34. Definition of Time and Value for Pseudo-Dynamic Analysis

The analysis determined the peak values of both the experimental data and the ANSYS model and then normalized these values based on the maximum values. Table 12 shows the p-values from the ANOVA for the effect of time for the factors of joist, subject, location and deflection of the three joist sizes tested. When comparing the different peak values with respect to time, the only factor with a significant influence was the joist used. This fact makes it difficult to generalize the results of the ANSYS model. However, it is important to recognize that only three joists were dynamically loaded and virtually simulated for the full model. Because the sample population is not representative does not mean the models are incorrect. An ANOVA conducted with a larger sample size could provide more accurate results for each joist type.

Table 12. p-Values for Effects of Time versus Joist, Subject, Location and Deflection on 'Time'

Joist Type	Joist	Subject	Location	Deflection
GP14	<0.001	0.301	0.876	0.243
GP12	0.001	0.283	0.977	0.081
TJI12	0.023	0.470	0.542	0.950

Table 13 shows the p-values from the ANOVA for the effect of value (deflection or rotation) upon the factors of joist, subject, location and deflection of the three joist sizes tested. As in Table 12, the joist values were significantly different as well as the subject and location for the TJI12 and the deflection for the GP14. Again, difference in the joist values may be due to the small sample size used for the full model. For the TJI, the spacing and subject showed significant differences also. These factors may indicate that greater sampling is needed to produce accurate results.

Table 13. p-Values for Effects of Value versus Joist, Subject, Location and Deflection on 'Value'

| Joist Type	Joist	Subject	Location	Deflection
GP14	<0.001	0.058	0.652	0.049
GP12	<0.001	0.071	0.205	0.464
TJI12	<0.001	0.038	0.031	0.156

The results from the simplified pseudo-dynamic analysis are presented in a graphical comparison form, which did not conform to any specific statistical test. The recorded deflections were graphed and grouped according to test subject, joist, location, and the type of deflection recorded. Each graph contained data from all joist testing replicates for each joist type, for a total of six different curves. The ANSYS model was also plotted and visually graded for goodness of fit. Ideally, the ANSYS model would fully encase the acquired data with only one or two peak values exceeding the curve created by the ANSYS model. Data from the first half of the joist was given more emphasis due to the dynamic effects in the second half of the joist not captured by the computer model. The graphs were visually rated one to five depending on how conservative or un-conservative the ANSYS model represented the acquired test data. Graphs were deemed either 1 for overly conservative or 5 for overly un-conservative. A value of 3 was assigned to those graphs that resembled the acquired data very well. The graphs were graded twice in a random order, to prevent any bias from a particular joist type. Figure 35 shows a graphical representation of grades 1, 3, and 5.
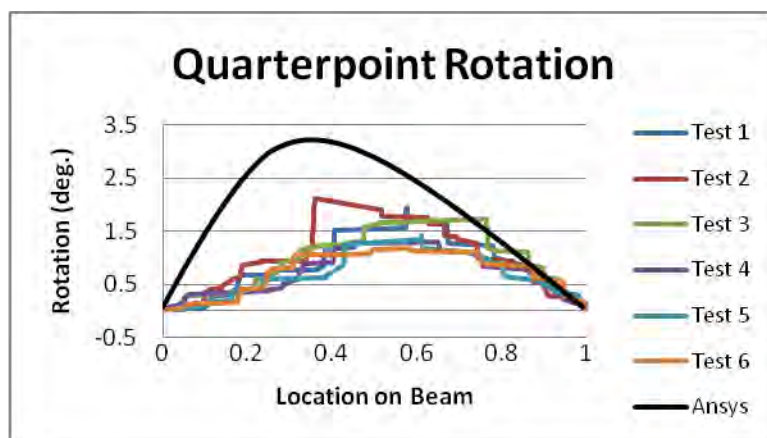
(a) Rating 1
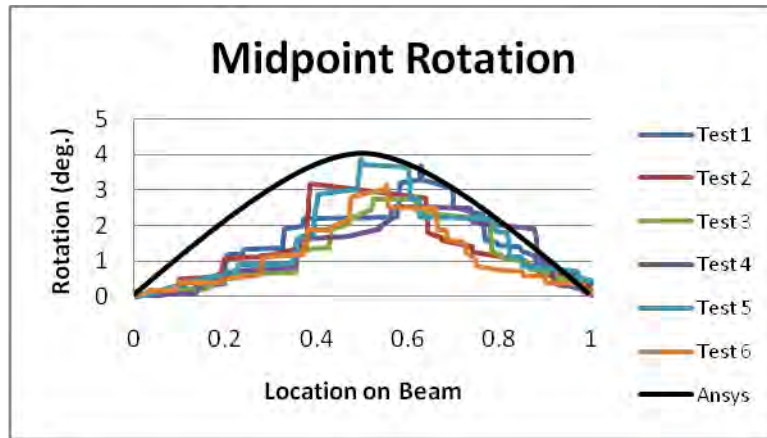
(b) Rating 3
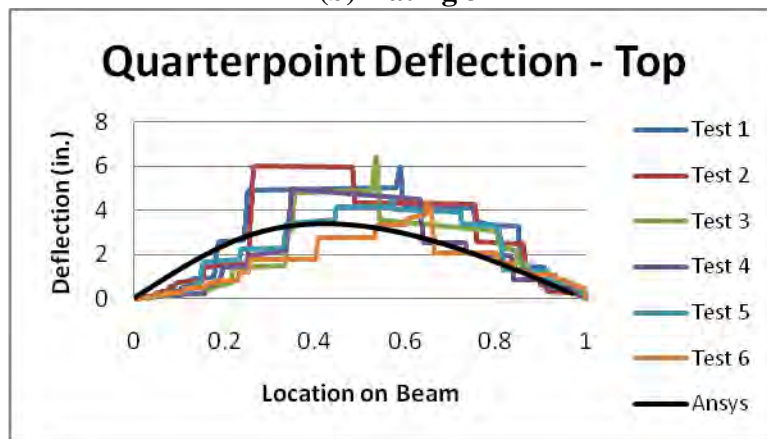
(c) Rating 5

Figure 35. Representations of Ratings used to Categorize Simplified Pseudo-Dynamic Graphs

Table 14 shows the average rating for each deflection measurement classified by joist type. Average values lower than 3.0, as in the GP14 and GP12, indicate that the model was slightly conservative, while the TJI12 joists had average values above 3.0, indicating that the model was non-conservative. The load values used in the ANSYS model were generated by using a constant percentage of the test subjects body weight for all three simplified models. From observing the results of the simplified analysis, future modeling may be more appropriate to relate the induced load to the length of the beam and the polar moment of inertia. There does not appear to be any effect on the location of the measurement and the applicability of the ANSYS model. The model predicted the bottom flange lateral deflection the best, followed by the rotation and then the top flange lateral displacement. This contrasts the results from the full pseudo-dynamic tests in which the order of the measurement type was reversed.

Table 14. Results from Simplified ANSYS Model

Joist Type	Midpoint			Quarter Point			Average
	Top Flange	Bottom Flange	Rotation	Top Flange	Bottom Flange	Rotation	
GP14	2.40	3.05	2.20	2.25	2.90	2.10	2.48
GP12	2.65	2.80	2.65	2.55	2.60	2.75	2.67
TJI12	3.20	3.30	3.40	3.25	3.10	4.10	3.39

Overall the finite element model was judged to be applicable to describe the lateral torsional buckling behavior of the GP14 and GP12 wood composite I-joists. The ANSYS model predicted the deflections of these beams to the midpoint of the beam within the 10 percent deviation limit. However, the variability in the numerous analytical comparisons indicates that the model does not represent the behavior of the TJI12 I-joists. The full pseudo-dynamic analysis indicated that the model deviated from the acquired test data almost immediately and the simplified analysis indicated that the model was un-conservative for all measurements.

Specific Aim #3

This section compared the different brace configurations to examine if the bracing behavior had a significant effect on the I-joist movement. Each dependent variable (lateral acceleration, lateral displacement and twist) was analyzed separately for significant differences. Then, some of the covariate factors were studied to determine the effect of participant static weight and occupation upon the joist movement.

Lateral Acceleration

The lateral acceleration data consisted of 350 data points: 200 data points for the 60 in. brace configuration and 150 data points for the 80 in. brace configuration. Table 25 shows the average values of the lateral accelerations for each brace stiffness at each brace configuration and the percent differences between each brace configuration. The 1.2 lb/in. stiffness had the largest percent difference between the two brace configurations, whereas the infinite stiffness had the smallest percent difference. Another important observation was the percent difference of the zero stiffness bracing. In theory, these values should be identical since they represented the I-joist acting without any bracing. Differences in acceleration between the two groups of test subjects that walked across the I-joist may have caused the 19.65% difference observed, demonstrating the variability of the test subjects themselves.

Table 15: Evaluation of Lateral Accelerations for Both Brace Configurations at Each Brace Stiffness

60 in. Brace Configuration		80 in. Brace Configuration		% Difference[1]
Stiffness (lb/in)	Average (ft/s^2)	Stiffness (lb/in)	Average (ft/s^2)	
0.0	18.366	0.0	22.858	19.65%
1.2	38.045	1.2	22.477	-69.25%
8.5	15.833	8.5	15.092	-4.90%
14.0	13.645	14.0	14.826	7.95%
∞	11.549	∞	11.742	1.66%

[1] % Difference = (80 in. – 60 in.) / 80 in. * 100%

Further comparisons for each point of interest were performed for each brace stiffness at each brace configuration. Figure 36 displays the distribution of lateral accelerations along the span of the I-joist. The "x" denotes the percentage of total length from the end support, so that an x/L of 0.5 corresponds to mid-span. In addition, the black vertical lines display where bracing was located. Figure 36 reveals that the 1.2 lb/in. brace stiffness behaved very different from the rest of the brace stiffness values. The spring stiffness combined with the I-joist's stiffness caused a frequency of walking near the I-joist's natural frequency, possibly causing greater lateral accelerations to occur. The other four brace stiffness (zero stiffness, 8.5 lb/in., 14.0 lb/in. and infinitely stiff) followed an inverse relationship between brace stiffness and lateral acceleration that was expected: As the brace stiffness increased, the lateral acceleration decreased. This trend can also be observed in Table 15. The only location along the I-joist where this trend does not occur is at position 0.125. This could have been due to the stiffness of the end support or test subjects may have caused larger lateral accelerations.
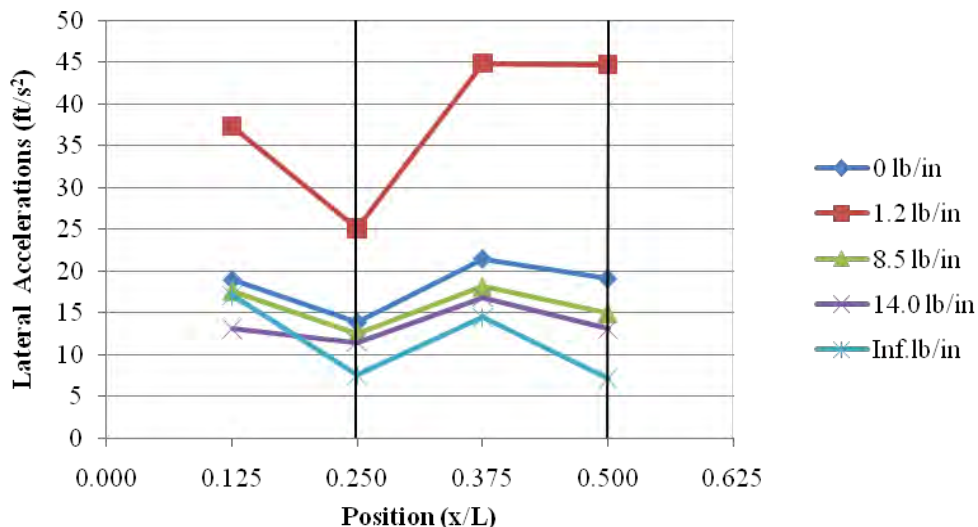

Figure 36: Lateral Accelerations for the 60 in. Brace Configuration

Figure 37 shows the results for the 80 in. brace configurations and is constructed the same as Figure 36. Figure 37 reveals the same trend described earlier - as brace stiffness increased, lateral accelerations decreased. However, for the 80 in. brace configuration, the 1.2

lb/in. brace stiffness followed this trend except at position 0.33. As in Figure 36, Figure 37 displayed an increase in lateral acceleration for the 1.2 lb/in. brace stiffness. The lateral accelerations of the other four brace stiffness decreased at the braced point. As noted earlier, this change in behavior could be due the combination of the brace stiffness and I-joist stiffness. For the two configurations, the infinitely stiff bracing obtained the lowest lateral accelerations with the exception of the 0.33 point.
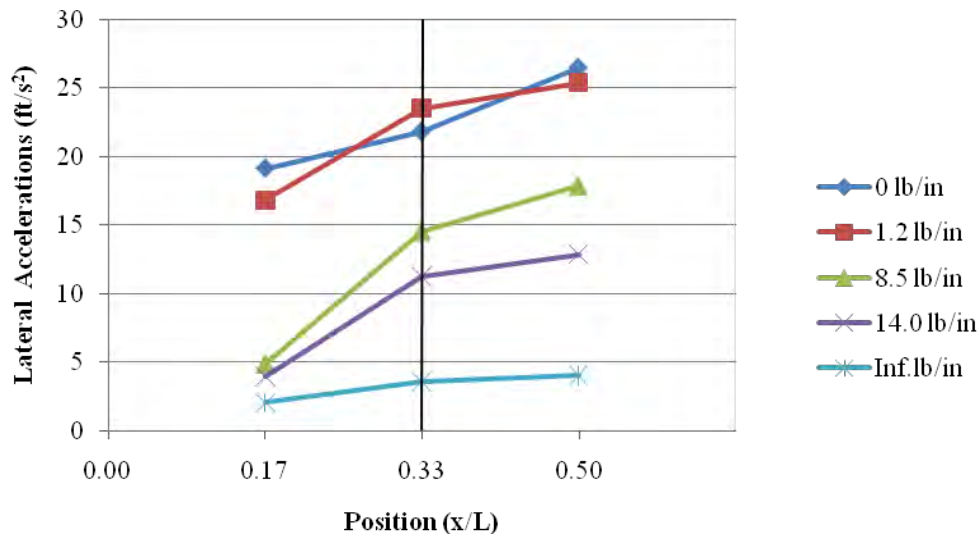

Figure 37: Lateral Accelerations for the 80 in. Brace Configuration

Lateral Displacements

Comparisons were performed for the lateral displacements of the I-joist, and the tables and graphs were constructed the same as the lateral accelerations. The lateral displacement data was extracted from the string potentiometers attached to the top flange. Table 16 displays the average of the lateral displacements for each bracing configuration, as well as the percent differences between them. The largest percent difference occurred for the 1.2 lb/in. brace stiffness, while the infinitely stiff brace stiffness had the second highest percent difference. Table 16 shows the same inverse relationship for both brace configurations between brace stiffness and lateral displacement - as brace stiffness increased, lateral displacement decreased. This relationship was expected and correlated with lateral stability and bracing fundamentals. The percent difference was approximately equal for the zero stiffness bracing for the two brace configurations.

Table 16: Evaluation of Lateral Displacements for Both Brace Configurations at Each Brace Stiffness

60 in. Brace Configuration		80 in. Brace Configuration		% Difference[1]
Stiffness (lb/in)	Average (in)	Stiffness (lb/in)	Average (in)	
0.0	1.332	0.0	1.327	-0.38%
1.2	0.847	1.2	0.988	14.26%
8.5	0.613	8.5	0.652	6.10%

| 14.0 | 0.548 | 14.0 | 0.542 | -1.17% |
| ∞ | 0.336 | ∞ | 0.364 | 7.66% |

[1] % Difference = (80 in. – 60 in.) / 80 in. * 100%

Figures 38 and 39 show the lateral displacements for the 80 in. and 60 in. bracing configurations, respectively. These figures were constructed in the same manner as the lateral acceleration graphs with respect to the x-axis orientation and the vertical lines denoting where bracing was located. Both graphs show the same trend as Table 16 - as brace stiffness increased, lateral displacement decreased. These graphs showed a parabolic relationship of the lateral displacement and location, and the largest lateral displacement occurred at mid-span. As the location nears the mid-span, the lateral displacement approached its maximum value with the slope of the lateral displacement-position graph approached zero. The lateral displacement behavior appeared to be symmetrical about the mid-span of the I-joist with a maximum value at mid-span.
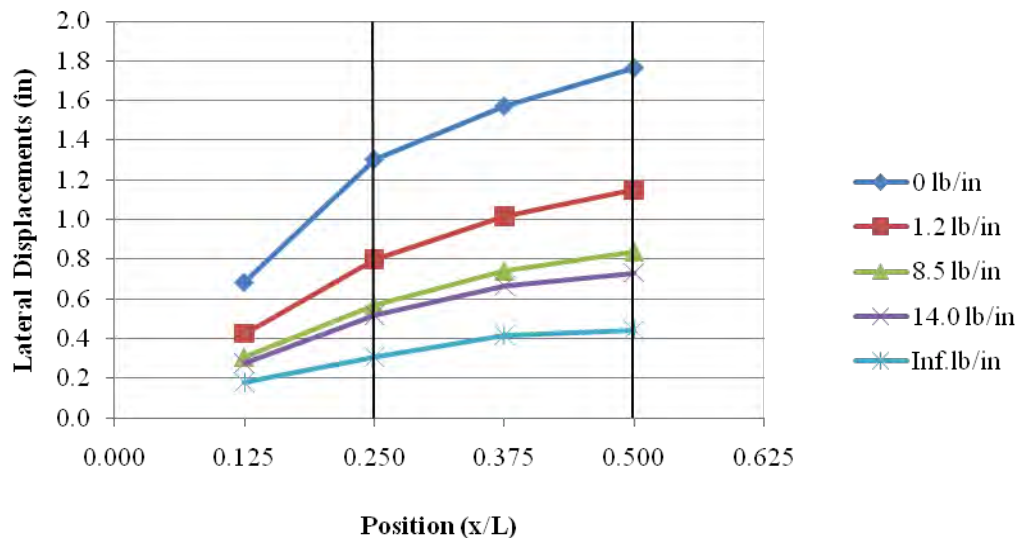

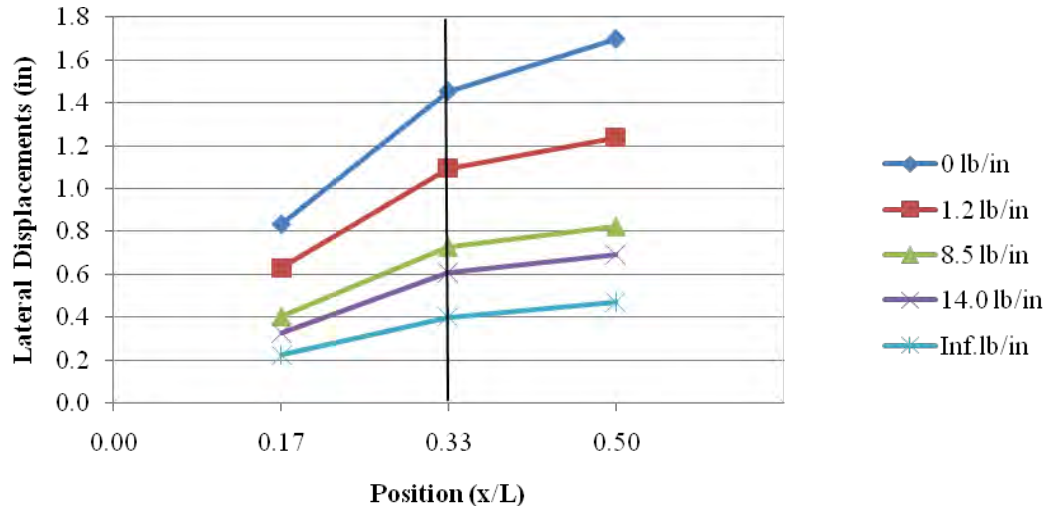**Figure 38: Lateral Displacements for the 60 in. Brace Configuration**

Figure 39: Lateral Displacements for the 80 in. Brace Configuration

Twist

The twist of the I-joist was calculated using the top flange and bottom flange string potentiometer data. Table 17 shows the averages of the twist for each bracing configuration, as well as the percent differences between the configurations. The largest percent difference occurred at the infinitely stiff bracing and the second largest percent difference occurred at the 1.2 lb/in. brace stiffness. None of the percent differences were negative, indicating that the 60 in. brace configuration always had a smaller twist than the 80 in. brace configuration. The 60 in. brace configuration had an increased amount of bracing causing reduced twist of the joist. The inverse relationship between brace stiffness and twist was also observed - as brace stiffness increased, twist decreased. This is a trend that was observed for all three dependent variables.

Table 17: Evaluation of Twist for Both Brace Configurations at Each Brace Stiffness

60 in. Brace Configuration		80 in. Brace Configuration		% Difference[1]
Stiffness (lb/in)	Average (deg)	Stiffness (lb/in)	Average (deg)	
0.0	3.364	0.0	3.790	11.24%
1.2	2.426	1.2	2.856	15.05%
8.5	1.960	8.5	2.165	9.46%
14.0	1.760	14.0	1.910	7.86%
∞	1.112	∞	1.370	18.84%

[1] % Difference = (80 in. – 60 in.) / 80 in. * 100%

Figures 40 and 41 show the twist values along the length of the beam for the 60 in. and 80 in. configurations, respectively. These figures show the same inverse relationship that Table 17 revealed: as brace stiffness increased, twist decreased. These graphs display a parabolic relationship between twist and position, with the maximum twist occurring at mid-span. For both configurations, the slope approached zero near mid-span indicating that the twist behavior was symmetrical about the mid-span of the I-joist.
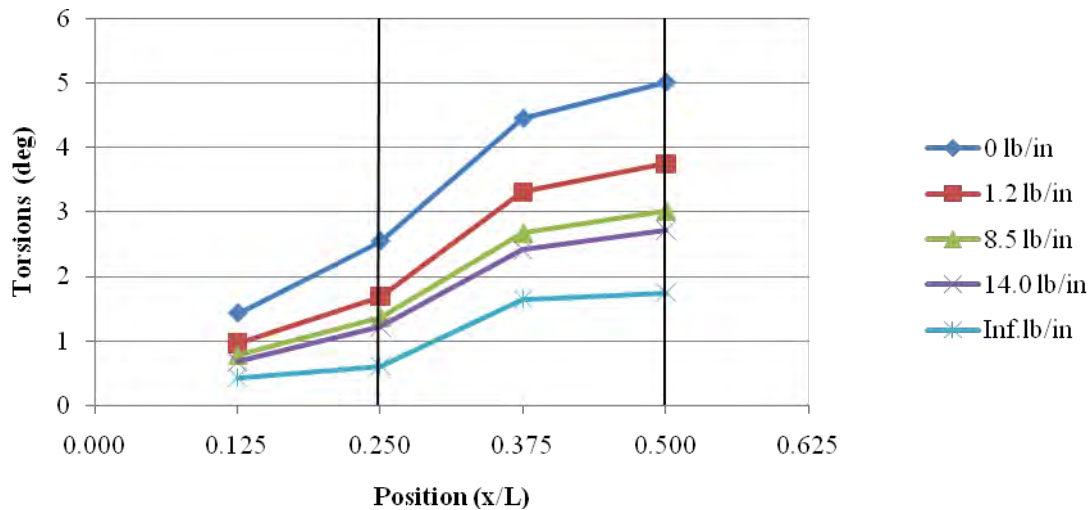
Figure 40: Twists for the 60 in. Brace Configuration
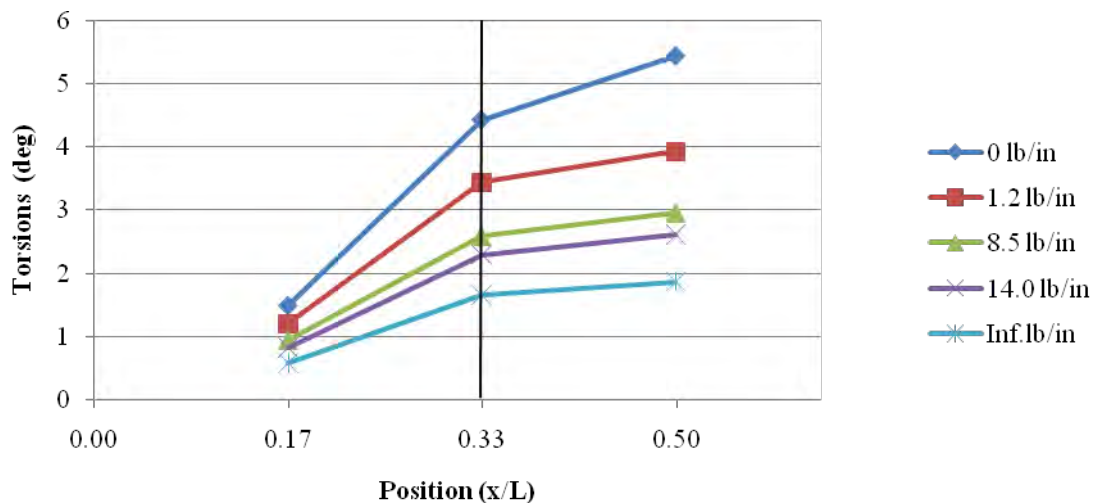
Figure 41: Twists for the 80 in. Brace Configuration

Comparison of Both Brace Configurations Using All Five Brace Stiffnesses

This section compared the two different brace configurations. All three dependent variables were analyzed separately for each brace configuration, and all five brace stiffness were analyzed together. Table 18 displays the results of the average maximum values of the lateral acceleration, lateral displacement and twist for each configuration as well as the percent difference and p-value from ANOVA comparison. The largest percent difference occurred between the two configurations for the twist, with lateral accelerations having a similar percent difference. The large percent difference between the two configurations was due to the difference in the 1.2 lb/in. brace stiffness values increasing the average of the 60 in. brace configuration. The percent difference of the lateral acceleration is negative, indicating that the 60 in. brace configuration had larger lateral accelerations, which was consistent with Figures 36 and 37. Brace configuration was not statistically significant for the lateral accelerations or lateral displacements, but was statistically significant for twist ($p = 0.016$). In addition, twist had the

62

largest positive percent difference between the two configurations. The greatest difference in the individual values was noticed for the twist

Table 18: Evaluation of Both Brace Configurations for all Brace Stiffness

Values	Lateral Acceleration	Lateral Displacement	Twist
60 in. Spacing Average	19.5 ft/s^2	0.735 in	2.124 deg.
80 in. Spacing Average	17.4 ft/s^2	0.775 in	2.418 deg.
% Difference [1]	-12.0%	5.09%	12.2%
p-value [2]	0.954	0.207	0.016

[1] % Difference = (80 in. – 60 in.) / 80 in. * 100%
[2] Significant p-values are highlighted.

Comparison of Both Brace Configurations at Each Brace Stiffness

The different brace configurations at each individual brace stiffness were compared. Table 19 displays the statistical analysis results for all three dependent variables. For lateral accelerations and twist, the 1.2 lb/in. brace stiffness was significantly different between the two brace configurations, and borderline for lateral displacements ($p = 0.053$). Infinitely stiff bracing was significantly different for lateral displacements and twist. As the brace stiffness approached infinity, increased stiffness significantly reduced the lateral displacement and twist. Since the twist had two significantly different values ($p < 0.05$), an increased amount of bracing does have a significant effect on reducing the twist caused by lateral buckling.

Table 19: Statistical Comparison of Both Brace Configurations at Each Brace Stiffness

Stiffness (lb/in)	Lateral Acceleration p-value	Lateral Displacement p-value	Twist p-value
0.0	0.360	0.940	0.567
1.2	0.012	0.053	0.018
8.5	0.928	0.262	0.079
14.0	0.272	0.708	0.118
∞	0.311	0.029	<0.001

[1] Significant results are highlighted.

Comparison of Brace Stiffness with Both Brace Configurations

In this section, a comparison of the lateral acceleration at and away from bracing points determined the role of bracing in the differences between the acceleration from the two brace configurations. Table 20 displays the acceleration at points of interest with and without bracing as well as the percent difference and p-value of the statistical comparison of the values. The 1.2 lb/in. brace stiffness had the lowest percent difference of -0.07% ($p = 0.994$), and the lateral accelerations were approximately equal. There was no difference between a point with bracing and a point without bracing for the 1.2 lb/in. brace stiffness. The zero stiffness, 8.5 lb/in. and 14.0 lb/in. brace stiffness all had percent differences approximately 15% different ($p > 0.05$). There were no significant differences between points with bracing and points without bracing for these three stiffness values.

The infinitely stiff bracing stiffness had the largest percent difference of 43.99% ($p < 0.001$). The infinitely stiff bracing did have a statistically significant effect on points with

bracing compared with points without bracing. The percent difference was positive, indicating that the lateral acceleration of points without bracing were greater than lateral acceleration of points with bracing. The same trend was observed for all stiffness values, excluding the 1.2 lb/in. brace stiffness. Bracing does reduce the lateral acceleration at points with bracing and may act to disperse the accelerations to the adjacent I-joist. The bracing elements could be absorbing energy from the I-joist's movement that decreased the lateral acceleration.

Table 20: Evaluation of Lateral Accelerations at Different Points of Interest for Each Brace Stiffness with Both Brace Configurations

Stiffness (lb/in)	Point of Interest	Lateral Accelerations (ft/s²)	% Difference[1]	p-Value
0.0	No Bracing	21.529	15.15%	0.145
0.0	Bracing	18.268		
1.2	No Bracing	30.119	-0.07%	0.994
1.2	Bracing	31.142		
8.5	No Bracing	16.411	14.44%	0.235
8.5	Bracing	14.039		
14.0	No Bracing	15.138	16.71%	0.082
14.0	Bracing	12.608		
∞	No Bracing	14.383	43.99%	< 0.001
∞	Bracing	8.058		

[1] % Difference = (No Bracing – Bracing) / No Bracing * 100%

Another important observation from Table 20 was the 1.2 lb/in. brace stiffness had a negative percent difference, so that points with bracing had a larger lateral acceleration than points without bracing. This behavior could be due to the energy of the spring inducing more energy in the I-joist than is being transferred to other I-joists. During the testing as the spring stiffness increased, the I-joists moved in relation to each other more. When the brace stiffness was lower (1.2 lb/in.), the two outside I-joists moved in the opposite lateral direction as the middle I-joist. This change in behavior may signify a different transfer of energy through the braces caused by the natural frequency of the joist system. For the 1.2 lb/in. brace stiffness, the springs were compressed and stretched more than the other bracing stiffness and providing more energy on the I-joist.

The amount of energy a spring possesses is directly related to the square of its deflection. Since the 1.2 lb/in. brace had more deflection than the other springs, more energy would have been applied to the I-joist. This increase in energy could have been the cause of the 1.2 lb/in. brace to have a greater affect on the lateral accelerations. Another assumption could be that the energy from the springs combined with the energy of the string potentiometers could have caused a harmonic motion which increased the amount of lateral acceleration.

Comparison of Both Brace Configurations for Each Brace Stiffness

Another comparison examined the lateral acceleration generated by the different stiffness at points of interest with and without bracing considering each individual brace configuration to examine if brace configuration affected the lateral acceleration. Table 21 displays the results for the 60 in. brace configuration. The infinitely stiff bracing had the largest percent difference of

53.49% ($p < 0.001$) and was significantly different between points of interest with and without bracing. The other four stiffness had percent differences that ranged from 15.03% to 23.06% ($p > 0.05$). The 1.2 lb/in. brace stiffness had a positive percent difference, indicating that points without bracing had higher lateral accelerations than the points with bracing. This correlates with Figure 36 which displays the largest lateral accelerations occurring at points without bracing. This finding differs from the previous section, indicating that the negative percent difference in Table 20 resulted from the 80 in. brace configuration as shown in Table 22.

Table 21: Evaluation of Lateral Accelerations at Different Points of Interest for the 60 in. Brace Configuration for Each Brace Stiffness (significant results are highlighted)

Stiffness (lb/in)	Point of Interest	Lateral Accelerations (ft/s^2)	% Difference[1]	p-Value
0.0	No Bracing	20.236	18.50%	0.072
0.0	Bracing	16.493		
1.2	No Bracing	41.135	15.03%	0.063
1.2	Bracing	34.951		
8.5	No Bracing	17.894	23.06%	0.097
8.5	Bracing	13.770		
14.0	No Bracing	15.010	18.20%	0.152
14.0	Bracing	12.280		
∞	No Bracing	15.764	53.49%	< 0.001
∞	Bracing	7.333		

[1] % Difference = (No Bracing – Bracing) / No Bracing * 100%

Table 22 displays the results of the 80 in. brace configuration for lateral acceleration at different points of interest and brace stiffness. The 1.2 lb/in. had a negative percent difference of -11.48% meaning that the points with bracing experienced larger lateral accelerations than points without bracing. This could be due the energy of the spring acting on the I-joist or the dynamic load creating a natural frequency in the braced system as explained in the previous section. The infinitely stiff brace stiffness had the largest percent difference of 26.88% ($p = 0.127$). No significance between the two groups of points for the 80 in. brace configuration was found. However, the points without bracing had larger lateral accelerations than points with bracing. This trend was also the case for the other four brace stiffness ($p > 0.05$). In conclusion, there was no significance between the points with and without bracing, but the points with bracing were smaller than points without bracing except for the 1.2 lb/in. brace stiffness at the 80 in. brace configuration.

Table 22: Evaluation of Lateral Accelerations at Different Points of Interest for the 80 in. Brace Configuration for Each Brace Stiffness

Stiffness (lb/in)	Point of Interest	Lateral Accelerations (ft/s^2)	% Difference[1]	p-Value
0.0	No Bracing	22.822	4.40%	0.858
0.0	Bracing	21.818		
1.2	No Bracing	21.206	-11.48%	0.374
1.2	Bracing	23.527		
8.5	No Bracing	14.925	2.30%	0.984
8.5	Bracing	14.583		
14.0	No Bracing	15.266	13.08%	0.543
14.0	Bracing	13.268		
∞	No Bracing	13.002	26.88%	0.127
∞	Bracing	9.508		

[1] % Difference – (No Bracing – Bracing) / No Bracing * 100%

Lateral Acceleration Compared to Zero Stiffness Behavior

       Table 23 displays the percent differences between each brace stiffness at a specified point of interest compared to the zero stiffness behavior, and the highlighted rows denote points with bracing. For the 1.2 lb/in. brace stiffness, all the percent differences were negative for the 60 in. brace configuration and negative at the point with bracing for the 80 in. brace configuration. The 1.2 lb/in. brace stiffness increased the lateral accelerations throughout the span of the I-joist for the 60 in. brace configuration and at the point with bracing for the 80 in. brace configuration. This correlates with Figures 36 and 37, which show similar behavior indicating that a natural frequency for this particular brace stiffness and configuration may have been found (Chopra 2007). For the 8.5 lb/in. brace stiffness, the percent difference increased as the position approached mid-span for the 60 in. brace configuration but stays almost constant throughout the span for the 80 in. brace configuration. The increased amount of bracing decreased the lateral accelerations by a greater magnitude as the position approached mid-span but decreased the lateral accelerations by about the same magnitude throughout the span with less bracing. The increased stiffness lead to reduced lateral accelerations.

Table 23: Evaluation of Lateral Accelerations at Specified Points of Interest for Each Brace Stiffness Relative to Zero Brace Stiffness

	Position (x/L)	Brace Stiffness (lb/in)			
		1.2	8.5	14.0	∞
60 in. Brace Config-uration	0.125	-96.93%	7.03%	30.69%	10.08%
	0.250	-81.44%	9.25%	17.17%	45.78%
	0.375	-108.86%	15.59%	21.53%	32.70%
	0.500	-133.99%	21.79%	31.63%	62.63%
80 in. Brace Config-uration	0.167	12.17%	35.90%	34.27%	33.78%
	0.333	-7.84%	33.16%	39.18%	56.42%
	0.500	4.16%	33.65%	32.25%	49.70%

[1] % Difference = (Zero Brace Stiffness – Brace Stiffness) / Zero Brace Stiffness * 100%

For the 14.0 lb/in. brace stiffness, the percent differences were sporadic for the 60 in. brace configuration, but were almost constant for the 80 in. brace configuration. The percent difference was greatest at the bracing location for the 80 in. brace configuration. The percent differences were larger for the 14.0 lb/in. brace stiffness than for the 8.5 lb/in. brace stiffness and revealed the same trend that has been observed throughout the analysis: as brace stiffness increased, lateral acceleration decreased. For the infinitely stiff brace stiffness, the percent differences were the largest at points with bracing. In addition, the percent differences were larger at most of the points of interest for the infinitely stiff brace stiffness than for the 14.0 lb/in. brace stiffness. The only location the percent differences were not greater was at the location closest to the support.

Table 24 displays the results of the statistical analysis, as well as the percent differences, to observe which brace stiffness had a significant affect on the I-joist's lateral acceleration relative to the zero stiff brace stiffness. For the 60 in. brace configuration, all four stiffness were statistically significant. The 1.2 lb/in. brace stiffness had the largest percent difference of -107.15%, so that the brace stiffness more than doubled the lateral accelerations relative to the zero stiffness. The other three brace stiffness percent differences increased as the stiffness increased and correlated with previous observations. For the 80 in. brace configuration, the 1.2 lb/in. brace stiffness had lowest percent difference of 2.55% and was the only stiffness that was not statistically significant ($p = 0.696$). The other three stiffness values were all statistically significant and reveal the same trend as the 60 in. brace configuration: as brace stiffness increased, lateral displacement decreased.

Table 24: Evaluation of Lateral Accelerations at Each Brace Stiffness Relative to Zero Brace Stiffness for Each Brace Configuration (significant results are highlighted)

Stiffness (lb/in)	60 in. Brace Configuration		80 in. Brace Configuration	
	p-Value	% Difference[1]	*p*-Value	% Difference[1]
1.2	< 0.001	-107.15%	0.696	2.55%

8.5	0.034	13.80%	0.001	34.13%
14.0	< 0.001	25.70%	< 0.001	35.07%
∞	< 0.001	37.12%	< 0.001	47.36%

[1] % Difference = (Zero Brace Stiffness – Brace Stiffness) / Zero Brace Stiffness * 100%

Lateral Displacement Compared to Zero Stiffness Behavior

Table 25 displays the percent differences for each brace stiffness at a specified point of interest to the zero stiffness behavior, and was constructed the same as Table 24. The percent differences were almost constant throughout the span for each brace stiffness and configuration. For the 60 in. brace configuration, the largest percent difference always occurred at position 0.250. For the 80 in. brace configuration, the largest percent difference occurred at position 0.167 except for the 1.2 lb/in. brace stiffness which occurred at position 0.500. The percent differences were about equal with the 60 in. brace configuration being slightly larger at each stiffness except for the 1.2 lb/in. brace stiffness. For the 1.2 lb/in. brace stiffness, the 60 in. brace configuration had much larger percent differences than for the 80 in. brace configuration. An increased amount of bracing reduced the amount of lateral displacement. As the stiffness increased, there was little difference between the two configurations. Another trend that was observed from Table 25 was that the percent difference increased as the brace stiffness increased, which was consistent throughout the span of the I-joist. This correlates with previous observations and can be observed in Figures 38 and 39.

Table 25: Evaluation of Lateral Displacements at Specified Points of Interest for Each Brace Stiffness Relative to Zero Brace Stiffness

	Position x/L	Brace Stiffness (lb/in)			
		1.2	8.5	14.0	∞
60 in. Brace Configuration	0.125	37.98%	55.20%	59.84%	73.79%
	0.250	38.79%	56.61%	60.25%	76.56%
	0.375	35.40%	52.97%	57.63%	73.64%
	0.500	34.97%	52.57%	58.58%	74.85%
80 in. Brace Configuration	0.167	24.43%	51.71%	60.90%	73.38%
	0.333	24.58%	49.80%	58.23%	72.38%
	0.500	26.97%	51.32%	59.18%	72.35%

[1] % Difference = (Zero Brace Stiffness – Brace Stiffness) / Zero Brace Stiffness * 100%

Table 26 displays the results of the twist values for the different brace stiffness compared relative to zero brace stiffness. All four brace stiffness values for both brace configurations were statistically significant and the percent differences increased as the brace stiffness increased and correlated with previous observations made from Table 25. In addition, all percent differences were larger for the 60 in. brace configuration at each stiffness and were much larger for the 1.2 lb/in. brace stiffness. The increased amount of bracing reduced lateral displacement but once the

stiffness increased, the amount of bracing did not have as large of an affect as the stiffness. Also, a trend was observed that was noted earlier: as the brace stiffness increased, the lateral displacement decreased. The stiffness of the brace controlled the magnitude of the lateral displacements. The reduction of lateral displacement was due to the brace being located on the compression flange. The compression flange is where lateral movement occurs, so bracing this section of the I-joist is crucial in reduction of movement (Hindman et al. 2005b).

Table 26: Evaluation of Lateral Displacements at Each Brace Stiffness Relative to Zero Brace Stiffness for Each Brace Configuration (significant results are highlighted)

Stiffness (lb/in)	60 in. Brace Configuration		80 in. Brace Configuration	
	p-Value	% Difference[1]	*p*-Value	% Difference[1]
1.2	< 0.001	36.42%	< 0.001	25.57%
8.5	< 0.001	54.02%	< 0.001	50.85%
14.0	< 0.001	58.87%	< 0.001	59.19%
∞	< 0.001	74.77%	< 0.001	72.58%

[1] % Difference = (Zero Brace Stiffness – Brace Stiffness) / Zero Brace Stiffness * 100%

Twist Compared to Zero Stiffness Behavior

Table 27 displays the percent differences for each brace stiffness at a specified point of interest relative to the zero brace stiffness behavior. Percent differences were larger for the 60 in. brace configuration than the 80 in. brace configuration for all four brace stiffness values and showed that an increased amount of bracing reduced the twist of the I-joist. The percent differences increased as the position approached mid-span for the 80 in. brace configuration. For the 60 in. brace configuration, the percent differences decreased as the position approached mid-span and had the greatest percent difference at position 0.250. This percent difference also occurred for the lateral displacements and could be due to increased stiffness closer to the support causing an increase in stiffness at the support or the load being transferred to adjacent I-joists and their end supports. Another common trend was that the percent differences increased as the stiffness increased. All of the percent differences were positive and alluded to the inverse relationship: as brace stiffness increased, twist decreased.

Table 27: Evaluation of Twist at Specified Points of Interest for Each Brace Stiffness Relative to Zero Brace Stiffness

	Position x/L	Brace Stiffness (lb/in)			
		1.2	8.5	14.0	∞
60 in. Brace Configuration	0.125	32.90%	45.42%	52.55%	69.59%
	0.250	33.73%	46.30%	51.87%	75.90%
	0.375	25.74%	40.04%	45.87%	63.00%
	0.500	25.35%	39.84%	45.77%	65.14%
80 in. Brace Configuration	0.167	19.40%	36.38%	44.99%	60.94%
	0.333	12.50%	41.57%	48.19%	62.57%
	0.500	27.86%	45.70%	52.01%	65.68%

[1] % Difference = (Zero Brace Stiffness – Brace Stiffness) / Zero Brace Stiffness * 100%

Table 28 displays the results of the statistical analysis as well as the percent differences between specified brace stiffness relative to zero brace stiffness. All four brace stiffnesses for both brace configurations were statistically significant. For both brace configurations, the percent difference increased as brace stiffness increased. This trend correlated with the lateral displacements in Table 27, and was due to bracing of the compression flange. By bracing the compression flange as the brace stiffness increased, the amount of lateral displacement and twist decreased.

Table 28: Evaluation of Twist at Each Brace Stiffness Relative to Zero Brace Stiffness for Each Brace Configuration (significant results are highlighted)

Stiffness (lb/in)	60 in. Brace Configuration		80 in. Brace Configuration	
	p-Value	% Difference[1]	p-Value	% Difference[1]
1.2	< 0.001	27.87%	< 0.001	24.64%
8.5	< 0.001	41.72%	< 0.001	42.87%
14.0	< 0.001	47.68%	< 0.001	49.60%
∞	< 0.001	66.94%	< 0.001	63.85%

[1] % Difference = (Zero Brace Stiffness – Brace Stiffness) / Zero Brace Stiffness * 100%

Test Subjects Weight Comparison

The test subjects' static weights were compared to the three mechanical behaviors. An analysis of covariance (ANCOVA) was completed to determine if the weight of a test subject affected the behavior of the I-joist. The test subjects' weights varied from 135 lbs to 218 lbs, with a majority of the subjects being approximately 180 lbs to 190 lbs. Lateral accelerations were not statistically significant ($p = 0.596$). However, lateral displacement and twist were statistically significant ($p = 0.027$ and $p = 0.022$, respectively). Weight had a significant affect on lateral displacements and twist but not on lateral accelerations. Figures 42, 43 and 44 display all the data gathered for all three mechanical behaviors graphed with the weight of each test subject. Each figure has a total of 350 data points.

Figure 42 displays the distribution of the lateral accelerations with respect to the test subjects' weights. The heavier test subjects had larger outlying points. These outlying points are from the 1.2 lb/in. brace stiffness at the 60 in. brace configuration. These outlying points were not sufficient enough to prove that weight has a significant affect on lateral acceleration since the rest of the data points do not vary much as the test subjects' weight's increase. In addition, Figure 43 displays the distribution of lateral displacements with respect to the test subjects' weights. As the test subjects' weight increased, the I-joist experienced larger lateral displacements. Figure 44 displays the distribution of twist with respect to the test subjects' weights and is almost identical to Figure 43. This increase in weight (load) caused greater lateral displacements and twist correlates with basic beam theory.
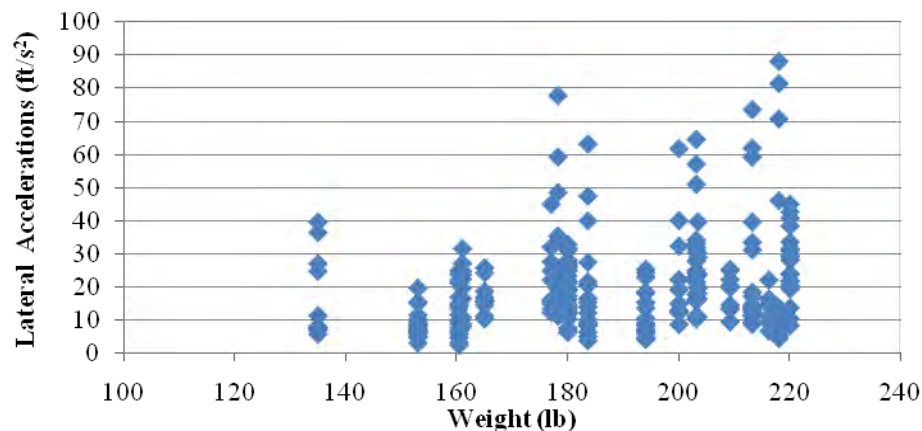

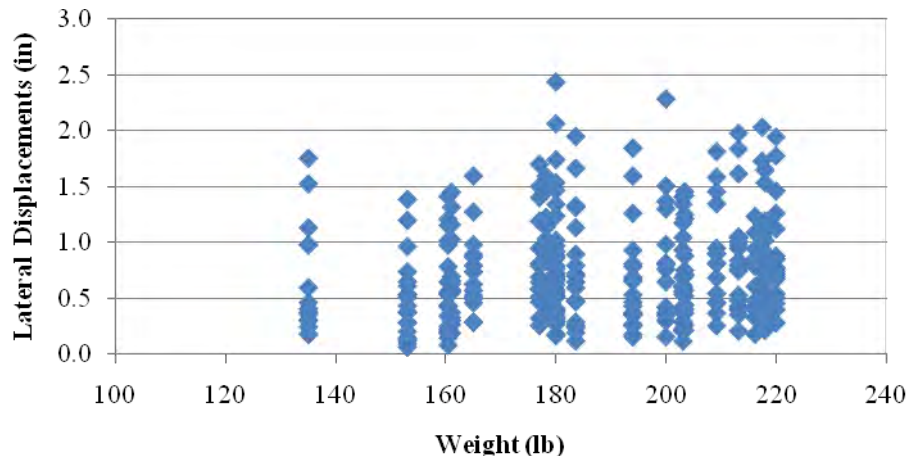**Figure 42: Comparison of Lateral Displacements and Subjects' Weight**

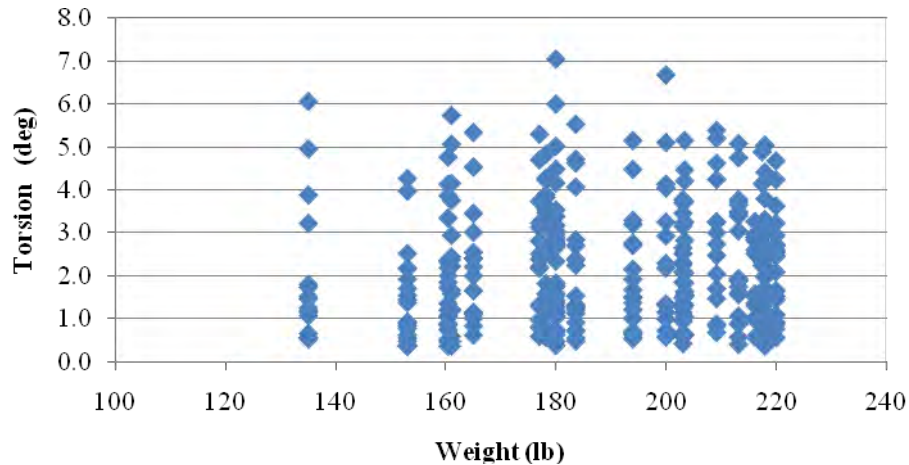**Figure 43: Comparison of Lateral Displacements and Subjects' Weight**

Figure 44: Comparison of Twist and Subjects' Weight

Test Subjects Occupation Comparison

Another comparison was performed which compared the three mechanical behaviors with respect to the subjects' occupation. The subjects' occupations were comprised of students and construction workers. Each test configuration had ten test subjects, consisting of seven students and three construction workers. This yielded a total of fourteen students and six construction workers for the entire experiment. Statistical analysis was performed and Table 30 displays the results. Table 30 showed that all three mechanical behaviors were not statistically significant ($p > 0.05$). However, lateral accelerations had percent difference of 24.71% which was much larger than the percent difference for lateral displacements and twist, 11.25% and 8.98%, respectively. This larger percent difference was due to the outlying points obtained from the 1.2 lb/in. brace stiffness for the 60 in. brace configuration. In addition, during testing one of the accelerometers failed and reduced the number of readings obtained for the construction workers. This reduction in the amount of data points, with a combination of small sample size, could have had an affect on the statistical analysis

Table 30: Evaluation of Test Subjects Occupation

	Lateral Accelerations (m/s^2)	Lateral Displacements (in)	Twists (deg)
Students	6.087	0.777	2.307
Construction Workers	4.583	0.689	2.100
% Difference[1]	24.71%	11.25%	8.98%
p-Value	0.179	0.300	0.208

[1] % Difference = (Students – Construction Workers) / Students * 100%

Further analysis showed differences between the two occupations with the students producing a greater magnitude for all three dependent variables. In addition, one important observation during testing was the construction workers felt more comfortable walking on the I-joists and did not have a problem walking to the beat of 45 beats per second produced by the metronome. However, the students showed a lack of comfort walking on the I-joists.

When a student began to lose their balance, they immediately grabbed the hand rails and did not walk to the beat. Some of the students said on the questionnaire that walking to the beat was the most difficult part of the experiment. They proclaimed it was difficult to concentrate on their balance and walking speed simultaneously. Some students wore construction boots and claimed these shoes provided them with more balance. Construction boots do provide more ankle support, but this could have been more psychological for the students who wore them. The construction workers produced smaller magnitudes for each dependent variable because they were more comfortable walking on the I-joists. Statistically there was no significant difference between students and construction workers, but there was a comparative difference between the averages of the two occupations.

Conclusions

The purpose of this project was to investigate the lateral buckling behavior of wood composite I-joists as a cause of falls from elevation. Specific aims included the observation and evaluation of static and dynamic loads, development of models to describe the lateral displacement and twist of the I-joists due to workers walking, and the development and testing of a temporary joist stabilizer method for establishing partial bracing of the I-joist studying variations of bracing stiffness and spacing.

Jobsite observations confirmed the need for workers to walk on unbraced I-joists. In many situations, workers were exposed to eccentric loading (carrying or handling heavy tools or materials) which could affect walking performance and lateral buckling. Modifications to the planned walking tests included the use of an eccentrically loaded tool belt on all participants to replicate this behavior. Static testing confirmed the small variability of I-joists at higher load-rotation stiffness. Dynamic loading demonstrated that a significant portion of lateral load is created by the action of workers walking on the beam, which lowers the vertical weight required to induce lateral buckling of the joist.

Modeling of the I-joist behavior used a pseudo-dynamic model incorporating the changing load as workers walked along the I-joist. Two of the three joist types were successfully modeled using this method. Simplification of the range of movement predicted by this method compared well to the experimental dynamic loading. This method provided a simpler method to describe lateral buckling for complex loading structures.

The effect of bracing caused a reduction in the lateral acceleration, lateral displacement and twist of the I-joists due to test subject's walking forces. For a low stiffness of 1.2 lb/in, adverse dynamic effects were noted, but all other bracing stiffness values showed a consistent performance. The bracing stiffness had a greater effect on reduction of joist movement than the brace spacing. The relationship between bracing stiffness and joist movement appears to be non-linear, with greater amounts of bracing stiffness causing a decreasing reduction in movement. Lateral displacement and twist of the joist increased as test subject weight increased, while the lateral acceleration did not.

References

Adair, C. and W. Camp. 2002. Market Outlook: Lumber, Structural Panels and Engineered Wood Products. Washington, DC, USA: APA - The Engineered Wood Association.

AF&PA. 2001. National Design Specification for Wood Construction. Washington, DC: American Forest and Paper Association. 173.

AF&PA. 2003. TR-14: Designing for Lateral Stability in Wood Members. 2003, American Forest and Paper Association. p. 37.

AF&PA. 1996. LRFD Load and Resistance Factor Design Manual for Engineered Wood Construction. 1996, Washington, DC: American Forest and Paper Association. 124.

Blosser, F. 2001. Strategic Precautions Against Fatal Falls On The Job Are Recommended By NIOSH, NIOSH, Editor.

Bureau of Labor Statistics. 2004a. Census of Fatal Occupational Injuries 2004 Data Information on Deadly Work Hazards, Department of Labor, Editor. p. 17.

Bureau of Labor Statistics. 2004b. Table A-9 Fatal Occupational Injuries by Event or Exposure and Major Private Industry Division, All United States 2004, Department of Labor, Editor. p. 5.

Bureau of Labor Statistics. 2004c. Table A-1 Fatal Occupational Injuries by Industry and Event or Exposure, All United States 2004, Deparmtnet of Labor, Editor. p. 25.

Burow, J.R. 2005. Lateral Stability Considerations for Composite Wood I-joists. M. S. Thesis. Pennsylvania State University: University Park, PA. p. 176.

Chopra, A. K. 2007. Dynamics of Structure: Theory and Applications to Earthquake Engineering. 3rd edition. New Jersey: Pearson Prentice Hall.

Donelan, J.M., et al. 2004. Mechanical and metabolic requirements for active lateral stabilization in human walking. Journal of Biomechanics. 37: p. 827-835.

Galambos, T.V. 1998. Guide to Stability Design Criteria for Metal Structures. 5th edition. New York, NY: John Wiley and Sons, Inc. 944.

Gard S.A. and Childress D.S. 2001. What Determines the Vertical Displacement of the Body During Normal Walking?. American Academy of Orthotists & Prosthetists, Vol. 13(3), pp. 64-67.

Hindman, D.P. 2003. Torsional rigidity and lateral stability of structural composite lumber and wood composite I-joists. Pennsylvania State University: University Park, PA. p. 222.

Hindman, D.P., H.B. Manbeck, and J.J. Janowiak. 2005a. Measurement and prediction of lateral torsional buckling loads of composite wood materials: Rectangular sections. Forest Products Journal, 55(9).

Hindman, D.P., H.B. Manbeck, and J.J. Janowiak. 2005b. Measurement and prediction of lateral torsional buckling loads of composite wood materials: I-joist sections. Forest Products Journal, 55(10).

Hooley, R.F. and B. Madsen. 1964. Lateral stability of glued laminated beams. ASCE-Journal of the Structural Division. 90(ST3): p. 201-218.

Hooley, R.F. and R.H. Duvall. 1972. Lateral buckling of simply supported glued laminated beams. Laminated Industry of Canada, Department of Civil Engineering, University of British Columbia.

Hsiao, H. and P.I. Simeonov. 2001. Preventing falls from roofs: a critical review. Ergonomics. 44(5): p. 537-561.

Huang M.H., Thambiratnam D.P. and Perera N.J. 2007 Dynamic Performance of Slender Suspension Footbridges under Eccentric Walking Dynamic Loads, Journal of Sound and Vibration, Vol. 303, pp. 239 – 254.

Huang, X. and J. Hinze. 2003. Analysis of Construction Worker Fall Accidents. Journal of construction engineering and management. 129(3): p. 262-271.

Hunting, K.L., et al. 1994. Surveillance of Construction Worker Injuries Through an Urban Emergency Department. Journal of occupational and environmental medicine / American College of Occupational and Environmental Medicine. 36(3): p. 356-364.

Janicak, C.A. 1997. Fall-Related Deaths in the Construction Industry. Journal of safety research. 29(1): p. 35-42.

Janowiak, J. J., D. P. Hindman and H. B. Manbeck. 2001. Orthotropic Behavior of Lumber Composite Materials. Wood and fiber science 33(4).

Kirby, P.A. and D.A. Nethercot. 1979. Design for Structural Stability. Constrado Monographs. Suffolk, United Kingdom: Granada Publishing Ltd.

Lipscomb, H.J., L. Li, and J.M. Dement. 2003. Falls among union carpenters. American journal of industrial medicine. 44(2): p. 148-56.

Lipscomb, H.J., J.M. Dement, and R. Behlman. 2003. Direct costs and patterns of injuries among residential carpenters, 1995-2000. Journal of occupational and environmental medicine / American College of Occupational and Environmental Medicine. 45(8): p. 875-80.

Maki, B.E., W.E. McIlroy, and S.D. Perry. 1996. Influence of Lateral Destabilization on Compensatory Stepping Responses. Journal of Biomechanics. 29(3): p. 343-353.

Nakamura S. and Kawasaki T. 2006 Lateral Vibration of Footbridges by Synchronous Walking, Journal of Constructional Steel Research, Vol. 62, pp. 1148 – 1160.

NIOSH. 1989. Preventing Worker Deaths and Injuries from Falls Through Skylights and Roof Openings, NIOSH, Editor. Department of Health and Human Services.

NIOSH. 2000. Worker Deaths by Falls: A Summary of Surveillance Findings and Investigative Case Reports, NIOSH, Editor. Department of Health and Human Services. p. 322.

Obata, T. and Y. Miyamori. 2006. Identification of a human walking force model based on dynamic monitoring data from pedestrian bridges. Computers and Structures. 84: p. 541-548.

OSHA. 1996. Issues in Labor Statistics, Department of Health and Human Services, Editor. 1996.

Pimentel R.L., Pavic A. and Waldron P. 2001. Evaluation of Design Requirements for Footbridges Excited by Vertical Forces from Walking, Canadian Journal Civil Engineering, Vol. 28, pp. 769 – 777.

Richardson, D.B., et al. 2004. Fatal Occupational Injury Rates in Southern and Non-Southern States, by Race and Hispanic Ethnicity. American journal of public health. 94(10): p. 1756-1761.

Rivara, F.P. and D.C. Thompson. 2000. Prevention of Falls in the Construction Industry: Evidence for Program Effectiveness. American journal of preventitive medicine. 18(4S): p. 23-26.

Shah, S.M.A., et al. 2003. Injuries and Illnesses from Wood Framing in Residential Construction, Washington State, 1993-1999. Journal of occupational and environmental medicine / American College of Occupational and Environmental Medicine. 45(11): p. 1171-1182.

Smulski, S. 1997. Engineered wood products, a guide for specifiers, designers and users. Madison, WI: PFS Research Foundation. 294.

Timoshenko, S. and J.M. Gere. 1961. Theory of Elastic Stability. 2nd edition. New York, NY: McGraw Hill Book Company.

Trus Joist. 2005. Specifiers Guide TJI 110 TJI 210 TJI 230 TJI 360 TJI 560 Joists. Vol. Number 2025. Boise, ID: Trus Joist, a Weyerhaeuser Business. 23.

Trus Joist. 2001. Specifiers Guide TJI/Pro 150, 250, 350 and 550 Joists. Boise ID: Trus Joist, a Weyerhaeuser Business. 23.

Trus Joist. 2001. Specifiers Guide TJI/Pro 120TS Joists. Boise, ID: Trus Joist, a Weyerhaeuser Business. 23.

Tirosh, O. and W.A. Sparrow. 2003. Identifying Heel Contact and Toe-Off Using Forceplate Thresholds With a Range of Digital-Filter Cutoff Frequencies. Journal of Applied Biomechanics. 19: p. 178-184.

USDA. 1999. Wood Handbook: Wood as an Engineering Material. Washington, DC: Forest Products Society.

Weyerhaeuser. 2004. Design Values for Structurwood® Panels. Technical Bulletin: Technical Updates G1401. Weyerhaeuser Company.

Zahn, J.J. 1992. Re-examination of Ylinen and other column equations. ASCE Journal of Structural Engineering. 118(10): p. 2716-2728.

Zhu, E.C., et al. 2005. Buckling of Oriented Strand Board Webbed Wood I-joists. Journal of Structural Engineering. 131(10): p. 1629-1636.

Publications

Journal Articles

Hindman, D. P., C. R. Bamberg, M. A. Nussbaum. 2010. Bracing of Wood Composite I-joists to Prevent Lateral Buckling Caused by Walking Loads. ASCE Journal of Materials. In Preparation.

Hindman, D. P., C. R. Bamberg, M. A. Nussbaum. 2010. Human Factors Contributing to Lateral Buckling Behavior of Wood Composite I-joists. Journal of Safety Research. In Preparation

Hindman, D. P., P. D. Timko, M. A. Nussbaum. 2010. Static and Dynamic Loading of Wood Composite I-joists Causing Lateral Buckling. Journal of Safety Research. In Preparation

Hindman, D. P., P. D. Timko, M. A. Nussbaum. 2010. Finite Element Modeling of Lateral Buckling of Wood Composite I-joists Under Walking Loads. Computers and Structures. In Preparation.

Proceedings

Hindman, D. P., C. R. Bamberg, P. D. Timko. 2010. Lateral Buckling of Wood Composite I-joists as a Mechanism Causing Falls from Elevation. 2010 International Conference on Fall Prevention and Protection. Morgantown, WV, May 18-20, 2010.

Kleiner, B., M. Nussbaum, T. Smith-Jackson, A. Songer, A. Nieto, T. Mills, R. Burdisso, D. P. Hindman, D. Young-Corbett, and M. Vorster. A socio-technical systems approach to innovation in construction safety and health: a formative evaluation. *Innovations Revealed: Institute of Industrial Engineers Annual Conference and Expo 2009*. Miami, FL. May 30-June 3, 2009.

Hindman, D. P. Lateral Buckling of Joists as a Cause of Falls from Elevation in Construction. *10th World Conference on Timber Engineering*. The Sheraton Resorts Phoenix Seagaia, Miyazaki, Japan. June 2-5, 2008.

Dissertation / Thesis

Bamberg, C. R. 2009. Lateral movement of unbraced wood composite I-joists exposed to dynamic walking loads. M. S. Thesis. Virginia Polytechnic Institute and State University. 78 p.

Timko, P. D. 2009. Finite element analysis of unbraced structural wood I-joists under construction loads. M. S. Thesis. Virginia Polytechnic Institute and State University. 87 p.

Inclusion of Gender and Minority Study Subjects

Ethnic Category	Female	Male	Sex/Gender Unknown or Not Reported	Total
Hispanic or Latino	0	2	0	2
Not Hispanic or Latino	0	31	0	31
Unknown (Individuals Not Reporting Ethnicity)	0	0	0	0
Ethnic Category: Total of All Subjects	0	33	0	33
Racial Categories				
American Indian / Alaska Native	0	0	0	0
Asian	0	4	0	4
Native Hawaiian or Other Pacific Islander	0	0	0	0
Black or African American	0	0	0	0
White	0	27	0	27
More Than One Race	0	0	0	0
Unknown or Not Reported	0	0	0	0
Racial Category: Total of All Subjects	0	31	0	31

This table differs significantly from the planned enrollment submitted at the beginning of the study. Originally, a female population and a larger Hispanic population were recommended. Due to change in the construction industry in the Southwest Virginia area, it was difficult to find construction workers to participate in these studies. In particular, the population of women working in construction trades is very small and the project was unsuccessful in recruiting them. The lack of diversity is hopefully tempered by the fact that the use of workers in this project was only to walk on the I-joists and provide a realistic loading. Subjects were not surveyed for any subjective measures.

Inclusion of Children

All subjects were over the age of 21. No children were included in this study.

Materials Available for Other Investigators

The theses written by C. Ryan Bamberg and Paul D. Timko which included much of the research from Specific Aim #2 and #3 are available electronically through the electronic thesis and dissertation (ETD) site at Virginia Tech (http://scholar.lib.vt.edu/theses/browse/). Other materials are available from Dr. Hindman by request.